

IMPRESSION - Prediction of NMR Parameters for 3-dimensional chemical structures using Machine Learning with near quantum chemical accuracy[†]

Will Gerrard, Lars A Bratholm, Martin Packer, Adrian J Mulholland, David R Glowacki*, Craig P Butts*

The IMPRESSION (Intelligent Machine PREdiction of Shift and Scalar information Of Nuclei) machine learning system provides an efficient and accurate method for the prediction of NMR parameters from 3-dimensional molecular structures. Here we demonstrate that machine learning predictions of NMR parameters, trained on quantum chemical computed values, can be as accurate as, but computationally much more efficient (tens of milliseconds per molecular structure) than, quantum chemical calculations (hours/days per molecular structure) starting from the same 3-dimensional structure. Training the machine learning system on quantum chemical predictions, rather than experimental data, circumvents the need for the existence of large, structurally diverse, error-free experimental databases and makes IMPRESSION applicable to solving 3-dimensional problems such as molecular conformation and stereoisomerism.

1 Introduction

NMR spectroscopy remains the pre-eminent analytical technique for elucidating molecular structure in solution, with the prediction and interpretation of ^1H and ^{13}C chemical shifts and scalar coupling constants playing a key role. The prediction of these parameters, especially in studies of 3-dimensional molecular structure, are increasingly moving towards quantitative comparison between computed values for proposed chemical structures and experiment. In such comparisons, the use of fast and accurate NMR prediction methods is crucial.

Fast empirical predictions of chemical shifts for 2-dimensional chemical structures have been used for decades, with the additivity rules exemplified by Pretsch¹ and HOSE-code² variants forming the basis of many analyses. However their applicability is limited by being based on 2-dimensional structures and cannot readily deal with 3-dimensional conformational or stereochemical analysis. Some modifications to treating 3-dimensional structures have been made by e.g. flat-but-stereochemically-aware HOSE codes³ or single conformer models of experimental systems⁴⁻⁶ but the improvements in 3-dimensional accuracy are limited as conformation and flexibility must necessarily be accounted for completely to achieve maximum accuracy. Multiple-bond ^1H - ^1H coupling constants are more directly linked to 3-dimensional structure, however generically applicable Karplus-style empirical relationships, such as the widely used equation reported by Haasnoot *et al*⁷, suffer from lower accuracy when confronted with complex chemical functionality while equations designed for spe-

cific sub-structures, e.g. carbohydrates⁸, are not applicable to the whole of chemical space. Finally, many NMR parameters, for example 1-bond ^1H - ^{13}C scalar coupling constants, $^1J_{\text{CH}}$, which are sensitive to both chemical connectivity *and* 3-dimensional structure are rarely used in isotropic studies precisely because there are no general fast predictive methods for $^1J_{\text{CH}}$.

For all of these reasons, the accurate prediction of NMR parameters in modern 3-dimensional structure determinations relies increasingly on the use of quantum chemical calculations, typically based on Density Functional Theory (DFT)⁹⁻¹². Optimal DFT methods can be accurate to within 1-2%, e.g. $^1J_{\text{CH}}$ predicted with <4Hz accuracy to experiment¹³⁻¹⁵ (on values that range from roughly 100-250Hz) and <0.2/<2ppm^{16,17} (on ranges of ~10/~200ppm) for $\delta^1\text{H}$ and $\delta^{13}\text{C}$ chemical shifts respectively. The substantial downside of DFT is the significant computation time required when using methods that can provide sufficient accuracy in NMR predictions. Accurate DFT-based predictions of chemical shift and scalar couplings typically take hours to days of CPU time for a single rigid molecule of even relatively low (~500) molecular mass. The largest proportion of this CPU time is occupied by the NMR computations, especially when computing scalar coupling constants. Naturally, in cases where multiple conformers or isomers must be considered (and thus predictions for multiple structures are required) this becomes days to months of computation for a single study.

Machine learning methods offer a solution to the time-demands of DFT NMR predictions, achieving them in seconds rather than hours or days. Such machines, trained on experimental data, for ^1H and ^{13}C chemical shifts based on 2-dimensional structures are well-established¹⁸⁻²¹. These systems are trained on hundreds of

[†]University of Bristol, Bristol

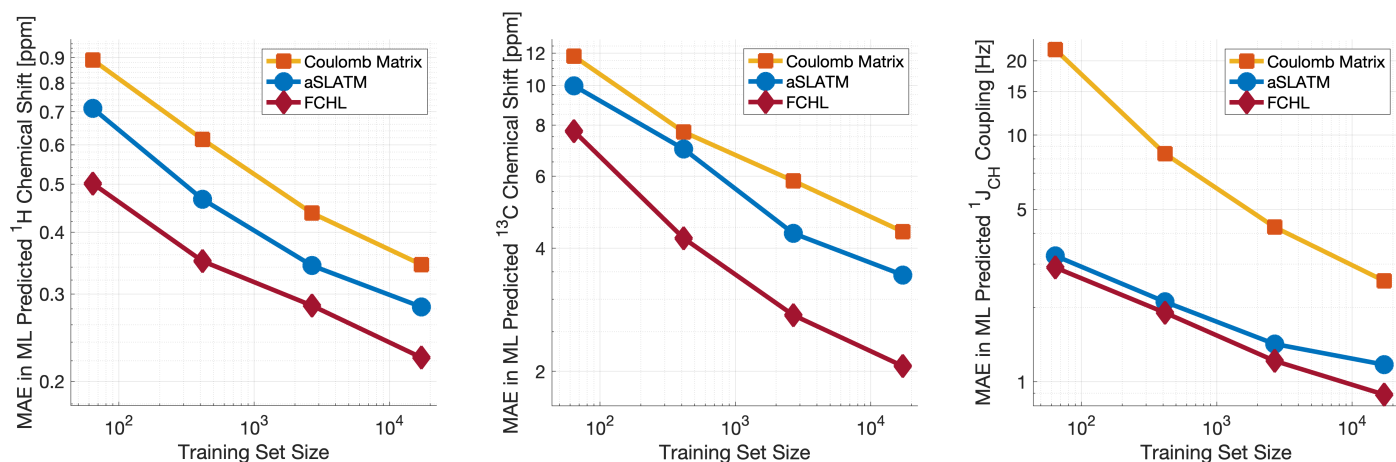


Fig. 1 Log-log plot of training set size vs the mean absolute error between ML predictions and DFT of the test set for $\delta^1\text{H}$ (left), $\delta^{13}\text{C}$ (centre) and $^1J_{\text{CH}}$ couplings (right). Results are shown for the Coulomb Matrix, aSLATM and FCHL kernel similarity measures.

thousands of validated experimental chemical shifts arising from tens of thousands of chemical structures. Training such machines for prediction of scalar couplings is more challenging because accurate and validated experimental databases do not exist on this scale (e.g. $^1J_{\text{CH}}$ values) and they can be critically dependent on 3-dimensional structure (e.g. $^3J_{\text{HH/CH}}$ values). On the other hand, a machine could be trained using large datasets of DFT-computed NMR parameters, such as chemical shifts and scalar couplings, derived from 3-dimensional structures. Such large DFT-derived datasets can be generated systematically with minimal effort and are not limited to offering accuracy only for structures that are similar to previously experimentally determined molecules. With a large enough training database, such a machine would be expected to approach the accuracy of DFT calculation of NMR parameters for 3-dimensional structure analysis, but with several orders of magnitude reduction in time for the NMR predictions. This approach was recently reported for solid-state chemical shift predictions by Paruzzo *et al* (SHIFTML²²), where the computational demand of DFT calculations on extended lattices are high and comparable to those needed for multi-conformer calculations on solution-state systems.

In this paper we describe the development of our first generation of solution-state NMR prediction machines - IMPRESSION (Intelligent Machine PREDiction of Shift and Scalar Information of Nuclei), trained on DFT-predicted values rather than relying on scarce or error-prone experimental data. We have chosen to demonstrate the versatility of machine learning of NMR parameters using both ^1H and ^{13}C chemical shifts and $^1J_{\text{CH}}$ couplings. We include scalar couplings in addition to chemical shift, as the former are less amenable to machine learning based on experimental data, and $^1J_{\text{CH}}$ precisely because it has been demonstrated to be valuable for elucidating both 2-dimensional connectivity and 3-dimensional structure^{5,23} but requires DFT to predict/interpret for most cases. Providing a fast and accurate predictive tool for $^1J_{\text{CH}}$ will be especially valuable and could encourage wider acceptance of this and other accessible NMR parameters in structure determinations. We demonstrate that IMPRESSION can pre-

dict all these NMR parameters for organic molecules, including 3-dimensional discrimination, with up to DFT accuracy but several orders of magnitude faster and can be applied to experimental data with comparable outcomes to DFT.

2 Results and discussion

2.1 Dataset production and framework

In order to train and test IMPRESSION, we developed a dataset of NMR parameters ($\delta^1\text{H}$, $\delta^{13}\text{C}$, $^1J_{\text{CH}}$), computed using DFT in the Gaussian09 software package²⁴. While more demanding computational methods could be considered²⁵, their computational cost would be extortionate with minimal improvement in outcomes for the training and testing datasets described. Instead we found that using *mPW1PW91/6-311g(d,p)* for optimisation and *wb97xd/6-311g(d,p)*²⁶⁻³⁰ for computing the NMR parameters was computationally efficient and sufficiently accurate for comparison to experimental values across a range of NMR parameters. In the geometry optimisations a tight optimisation criteria and ultrafine integral grids were used to minimise molecular orientation affecting geometries and energies (see reference³¹ and references therein for a discussion of this). The NMR parameters were calculated using gauge independent atomic orbitals with uncontracted basis sets to improve descriptions of the core orbitals³⁰ and calculation of all components of the scalar couplings (Fermi contact, spin dipole, diamagnetic spin orbit, paramagnetic spin orbit). The calculated magnetic shielding tensors were converted into chemical shifts using the linear scaling method and reference compounds reported by Tantillo *et al*^{10,32}. A training set of 882 structures (17,222 $^1J_{\text{CH}}$; 18,383 $\delta^1\text{H}$; 17,081 $\delta^{13}\text{C}$ values/environments) were selected by an adaptive sampling (active learning) procedure³³⁻³⁵ from a superset of 75,382 chemical structures comprising only C, H, N, O and F atoms in the Cambridge Structural Database³⁶ (accessed 7/9/2018). The adaptive sampling procedure trains an initial IMPRESSION machine from 100 chemical structures and then uses this machine to predict the parameters for all remaining structures in the superset to measure their variance in a 5-fold cross validation (*i.e.* how

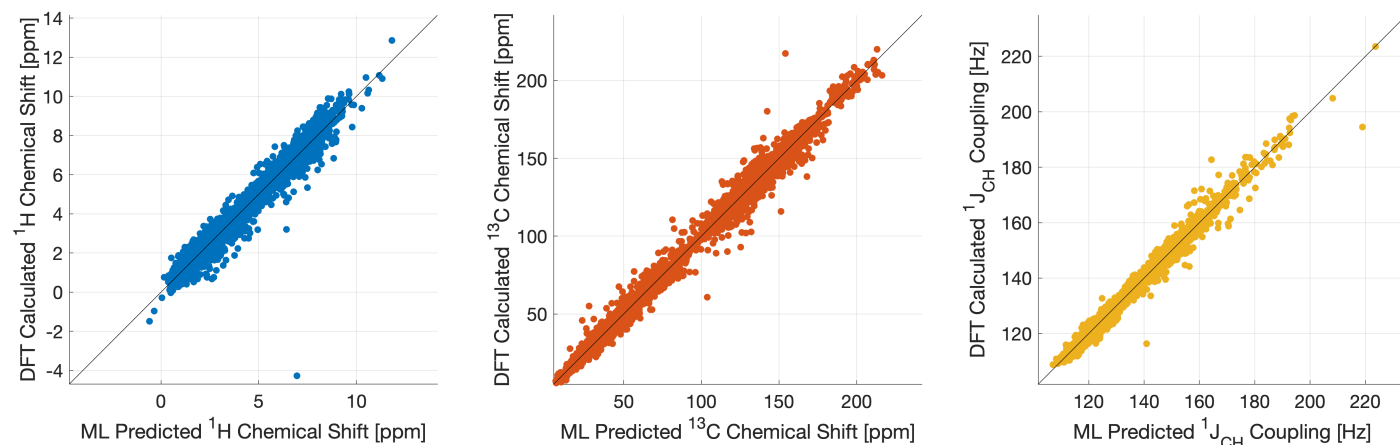


Fig. 2 IMPRESSION machine learning predictions compared to DFT computed NMR parameters for $\delta^1\text{H}$ (left), $\delta^{13}\text{C}$ (centre) and $^1J_{\text{CH}}$ couplings (right) without variance filtering.

much a given parameter changes when predicted from 5 separate machines each trained on a different 80% subset of the current training set). The 100 structures in the superset which show the highest variance are then added to the training dataset and the cycle is iterated (see supplementary information for further details). Adaptive sampling therefore adds the 100 structures at each training iteration which IMPRESSION is the most uncertain about. In doing so, each added structure provides the maximum benefit to the machine and substantially reduces the overall computational cost required to reach a given accuracy. The test set, against which the quality of the IMPRESSION predictions is independently tested, was comprised of a further 410 chemical structures (7788 $^1J_{\text{CH}}$; 7832 $\delta^1\text{H}$; 7522 $\delta^{13}\text{C}$ environments) harvested from the CSD-500 dataset recently reported by Paruzzo *et al.*²²

IMPRESSION uses a Kernel Ridge Regression³⁷ (KRR) framework to learn the $^1J_{\text{CH}}$ scalar couplings and ^{13}C and ^1H chemical shifts of molecular structures. KRR was successfully used by Paruzzo *et al.* to develop SHIFTML²². Neural networks have also been used to predict chemical shifts in small molecules from experimental data^{6,38,39}, however we found no clear advantages in using feed forward neural networks in this work as the accuracy was comparable to KRR for the datasets used, with the kernel methods being much faster to train with the given training set size. In order to encode the similarity between chemical environments of each molecular structure we tested three approaches previously described - Coulomb matrices⁴⁰, aSLATM⁴¹ and FCHL⁴², all available from the QML python package⁴³. We refer the reader to section S1.1 in the supplementary information and the respective papers describing each representation for more details. All of these kernel similarity measures compare *atomic* environments, so in the case of $^1J_{\text{CH}}$, we used the product of the separately calculated kernel similarities for the ^1H and ^{13}C nuclei as this performed better than either atomic environment alone. The KRR procedure is further described in the supplementary information (section S1.1).

Both aSLATM and FCHL were found to outperform Coulomb matrices (Figure 1), which is expected as Coulomb matrices only

include 2-body interactions, while aSLATM and FCHL both include three-body interactions as well. As FCHL provided the best performance for all three parameters and was substantially more computationally efficient than aSLATM, it was used in the final development of the full IMPRESSION machine.

2.2 Performance relative to DFT

During training, the machine performance for prediction of all NMR parameters ($\delta^1\text{H}$, $\delta^{13}\text{C}$, $^1J_{\text{CH}}$) improved steadily with increasing training set size, as illustrated in the learning curves (Figure 1). This indicates that the accuracy of the machine can be further improved by adding additional training data, however the absolute gains become marginal beyond the dataset size used here with a ten-fold increase in training set size approximately halving the average error between IMPRESSION and DFT. After training on the full set of 882 chemical structures, IMPRESSION predictions achieved mean absolute errors (MAE) of 0.23ppm/2.45ppm/0.87Hz for $\delta^1\text{H}/\delta^{13}\text{C}/^1J_{\text{CH}}$ predictions and root mean squared error (RMSE) of 0.35ppm/3.88ppm/1.39Hz against the independent test set (Figure 2).

Notably however, a very small number of predictions for the test set were much less reliable. For example, 186 (~2.3%) of the $\delta^1\text{H}$ values had errors >1ppm between IMPRESSION and DFT, with a maximum error (MaxE) of 11.22ppm. Similar outcomes were observed for the other parameters with 187 $\delta^{13}\text{C}$ values (~2.5%) with errors >10ppm (MaxE = 63.33ppm) and 14 (~0.2%) of the 7788 $^1J_{\text{CH}}$ predicted $^1J_{\text{CH}}$ values having errors of >10Hz (MaxE = 24.63Hz). Diagrams of the structures containing the five most significant outliers for each NMR parameter are shown in figures S19, S20, and S21 in the SI. Examination of the chemical environments of the most significant outliers show that they arise from unusual functional groups such as those containing sp-hybridised atoms, or unusual 3-dimensional environments such as atoms near pi-systems of aromatic rings. These outliers suggest that, as desired, the machine learning system is indeed very sensitive to the 3-dimensional relationships of the atoms in the structure. However this same sensitivity also makes IMPRESSION less accurate for chemical environments which are not very

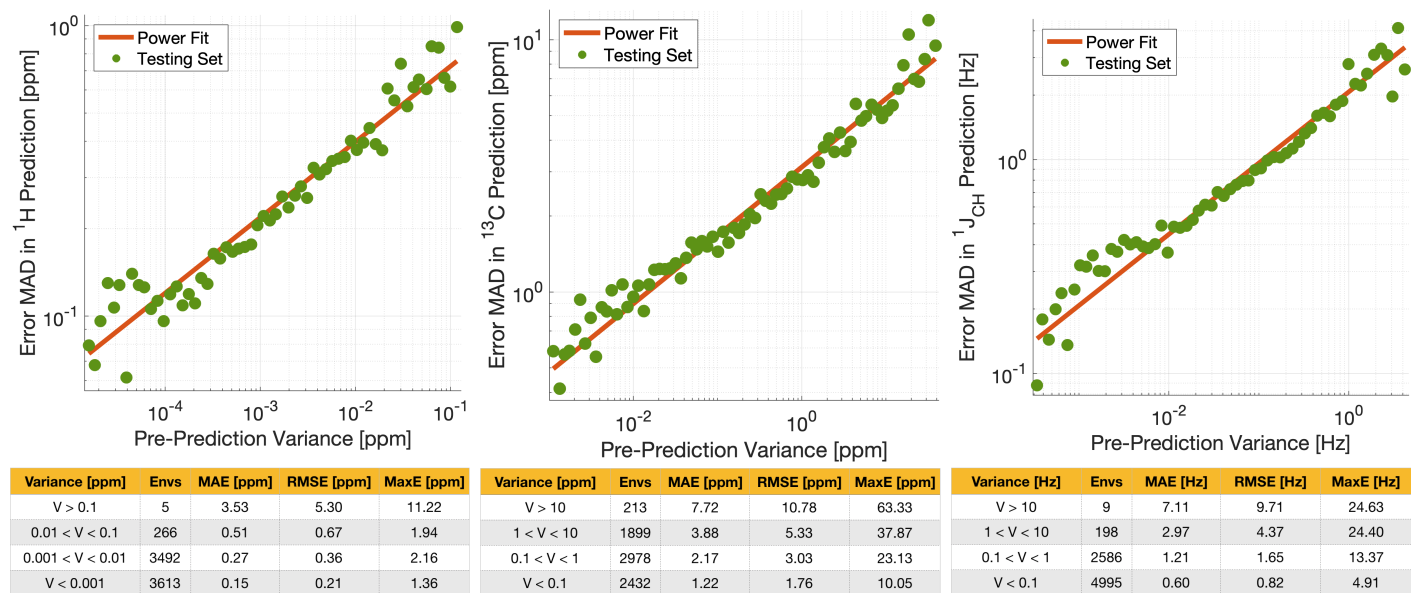


Fig. 3 Top: correlation between pre-prediction variance and prediction error between DFT and IMPRESSION for $\delta^1\text{H}$ (left), $\delta^{13}\text{C}$ (centre) and $^1J_{\text{CH}}$ couplings (right) on the test set. The prediction errors were binned by variance and an average error (MAE) was produced for each bin. Bottom: error metrics for different variance ranges.

similar to environments across the 882 molecular structures used to train IMPRESSION.

Crucially, we are able to *a priori* identify poorly described environments using the same variance-based approach used to generate the training set. By assessing the variance in the prediction of a given NMR parameter across a 5-fold cross-validation, we can quantify our confidence in each individual prediction since environments which are poorly described by the chemical structures in the training set will have high variance in this cross-validation. There is indeed a clear correlation of variance against prediction error for the independent test set (Figure 3). The tables in Figure 3 suggest that the bulk of the environments are predicted very accurately, and that the high variance environments are the dominant source of the large outliers.

In principle, removing IMPRESSION-predicted values which show high variances in cross-validation should provide a "pre-prediction variance filter" that will substantially improve the quality of, and thus the confidence in, IMPRESSION predictions. Selecting an appropriate variance cut-off for each NMR parameter is then simply a balance between desired prediction quality and the number of predictions which will be excluded by that cut-off. Reports of DFT accuracy with respect to experiment for $\delta^1\text{H}$ and $\delta^{13}\text{C}$ chemical shift predictions vary significantly, but typically in the range of 0.2-0.4ppm/2-4ppm, with the best reported accuracies down to <0.2/<2ppm^{16,17} in optimal cases. Similarly, Buevich *et al* recently highlighted that current best-in-class DFT methods predict $^1J_{\text{CH}}$ experimental values with accuracies of 2-4Hz, when presenting an optimised workflow for calculating $^1J_{\text{CH}}$ values which achieved an RMSE of 1.61Hz.

We therefore identified variance cut-offs for IMPRESSION predictions that provide a good compromise between accuracy and excluded values for the test set, which were found to be 1Hz for $^1J_{\text{CH}}$, 0.1ppm for $\delta^1\text{H}$ and 5ppm for $\delta^{13}\text{C}$. Applying these

pre-variance filter values improves the fits between IMPRESSION and DFT to levels that are comparable with literature reports for MAE/RMSE of DFT vs experiment (MaxE is rarely reported for large experimental validations, but the reader can find comparators from our experimental validations described below in section 2.3). For $\delta^1\text{H}$ the 0.1ppm filter excludes 5 environments (<0.1%) and improves the fit to MAE = 0.23ppm, RMSE = 0.32ppm; MaxE = 2.16ppm. For $\delta^{13}\text{C}$ a 5ppm filter provided a good fit MAE = 2.17ppm; RMSE = 3.25ppm; MaxE = 37.87ppm while excluding 538 (~7.2%) of the environments. For $^1J_{\text{CH}}$ a 1Hz filter improved the fit to MAE = 0.81Hz, RMSE = 1.17Hz; MaxE = 13.37Hz while discarding only 207 (<3%) of the environments.

As highlighted by the learning curves, further improvement to the machine predictions of DFT NMR results can be made by increasing size of the DFT-derived training dataset by around an order of magnitude. However at this stage variance-filtered IMPRESSION compares well enough with respect to DFT that it was taken forward. It should also be noted at this point that IMPRESSION only accelerates NMR prediction, it does not accelerate the 3D structure generation by DFT (which can still take hours/days). This overall time, *i.e.* 3D structure generation + NMR prediction, could be reduced further by using 3D structures derived from molecular mechanics rather than DFT. While not the key focus here, the use of molecular mechanics structures as inputs to a re-trained IMPRESSION machine was explored. While practical, this resulted in a ~30-50% increase in the average prediction errors for $\delta^1\text{H}$ and $^1J_{\text{CH}}$ presumably arising from a mismatch between the detail of molecular mechanics geometries and those used to calculate the DFT NMR parameters (see Section S2 in the SI for details). Interestingly, $\delta^{13}\text{C}$ predictions were relatively insensitive to this change, perhaps reflecting better description of carbon environments by molecular mechanics forcefields. This is an exciting avenue to explore further, but to focus the discussion here on

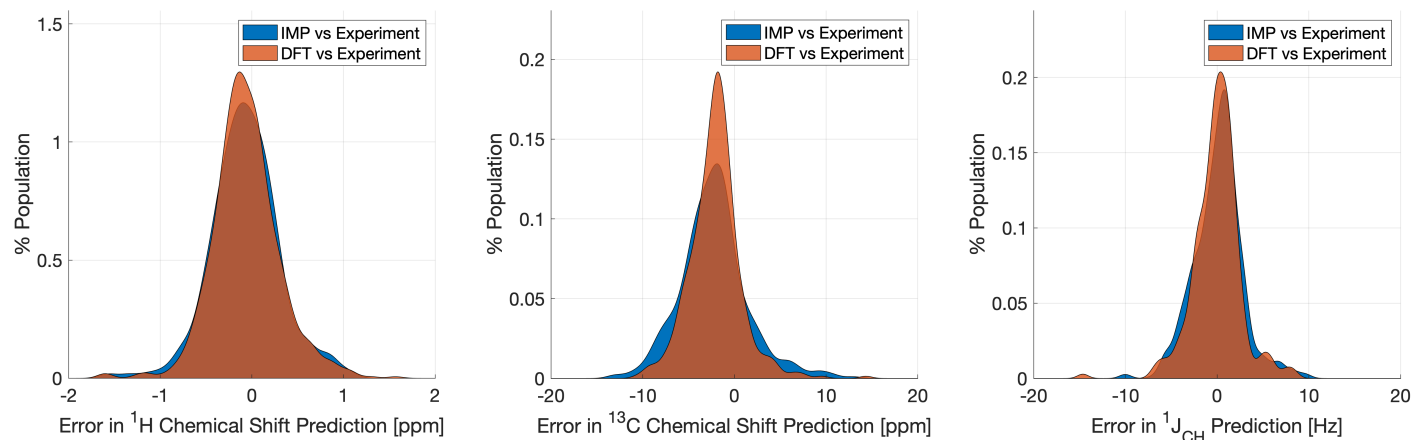


Fig. 4 Distribution of errors for machine learning NMR predictions and DFT calculations when compared to the relevant experimental validation dataset for $\delta^1\text{H}$ (left), $\delta^{13}\text{C}$ (centre) and $^1J_{\text{CH}}$ couplings (right). Variance filters applied to IMPRESSION predictions: $\delta^1\text{H} = 0.1\text{ppm}$ (0 of 734 environments removed), $\delta^{13}\text{C} = 5\text{ppm}$ (24 of 457 environments removed), $^1J_{\text{CH}} = 1\text{Hz}$ (143 of 608 environments removed).

the ability of IMPRESSION to reproduce DFT NMR predictions, the subsequent experimental comparisons are based on the IMPRESSION machine trained on the same DFT-geometries used for the DFT NMR predictions.

2.3 Performance relative to experiment

Naturally, a key test of IMPRESSION is its ability to reproduce DFT predictions of experimental values of relevant compounds. To test this for $^1J_{\text{CH}}$, a validation set of 608 experimental $^1J_{\text{CH}}$ values were taken from structures collated by Venkata *et al*²³ which contain C, H, N, O and F elements only. Firstly, we checked the ability of our $\omega\text{b97xd}/6\text{-}311\text{g(d,p)}$ DFT method itself to reproduce these experimental results. It should be noted in the subsequent analysis that all DFT and IMPRESSION predictions were based on the single conformers that Venkata *et al* reported for each compound. While not making the predictions entirely experimentally relevant, it allows direct comparison between DFT and IMPRESSION NMR predictions for this data. Calculating the 608 couplings with $\omega\text{b97xd}/6\text{-}311\text{g(d,p)}$ took 156 CPU hours and initially gave a relatively poor fit to experiment (MAE = 10.92Hz) but with a systematic offset from the experimental data by an average of -10.91Hz. Adding this systematic offset to the DFT-predicted values provided a good fit between DFT and experiment (MAE = 2.16Hz; RMSE = 3.33Hz; MaxE = 20.05Hz) and this was used for all subsequent comparisons to experiment based on this DFT method. As IMPRESSION is trained on DFT data computed with this same $\omega\text{b97xd}/6\text{-}311\text{g(d,p)}$ method and both methods use only single conformer predictions for each molecule, then these statistics represent a practical limit for the accuracy that we might expect from IMPRESSION on this experimental data.

IMPRESSION took only 60 CPU seconds to predict the full set of 612 $^1J_{\text{CH}}$ values but with some substantial outliers (MAE = 4.52Hz; RMSE = 10.49Hz; MaxE = 120.3Hz). Applying the 1Hz variance filter gave: MAE = 2.01Hz, RMSE = 2.69Hz, MaxE = 10.01Hz (removing 143 values) which was essentially identical accuracy to that obtained from the DFT method for these same

filtered environments: MAE = 1.83Hz, RMSE = 2.60Hz, MaxE = 14.63Hz. An overlay of the error distributions for DFT and the 1Hz variance-filtered IMPRESSION vs the experimental values (Figure 4) demonstrates the comparability between machine learning and DFT for $^1J_{\text{CH}}$ predictions. This represents quite excellent performance of the machine for reproducing experimental data in just a few seconds, with quality for the majority of environments as good as the best MAEs (1.5-4Hz) described by Buevich *et al* as typical for DFT methods, with <25% of the values being tagged as unreliable by the variance filter. Of course, if a slight loss in prediction quality is acceptable for a given study, then more predicted values could be retained by using a slightly looser variance-filter.

Similar accuracy could be obtained for IMPRESSION predictions of 734 ^1H chemical shifts for 36 structures reported by Smith and Goodman⁴⁴ in their DP4 dataset (again, single conformers were used for both DFT and IMPRESSION predictions). IMPRESSION predictions gave MAE = 0.29ppm, RMSE = 0.38ppm, MaxE = 1.59ppm, variance filter 0.1ppm but in this case no environments were lost to the variance filter and provided essentially the same outcomes as the $\omega\text{b97xd}/6\text{-}311\text{g(d,p)}$ DFT method on the same single conformer structures (MAE = 0.28ppm, RMSE 0.37ppm, MaxE 1.62ppm, see Figure 4 for an overlay of errors). The IMPRESSION predictions for $\delta^{13}\text{C}$ using the 5ppm variance filter identified during training and testing of the machine compared slightly less well to the DP4 experimental dataset (MAE = 3.44ppm, RMSE = 4.30ppm, MaxE = 13.06ppm, removing 24 environments) than DFT (MAE = 2.78ppm, RMSE = 3.48ppm, MaxE = 14.33ppm). A tighter 1ppm variance filter for the $\delta^{13}\text{C}$ predictions was examined, but gave only a slight improvement in prediction quality MAE = 3.20ppm, RMSE = 4.00ppm, MaxE = 13.03ppm while removing 120 out of the 458 carbon environments.

At every stage in this study we found that the IMPRESSION $\delta^{13}\text{C}$ predictions have a wider distribution of errors than the other NMR parameters when compared to the quality of the DFT from which they are trained. This is unsurprising given that the struc-

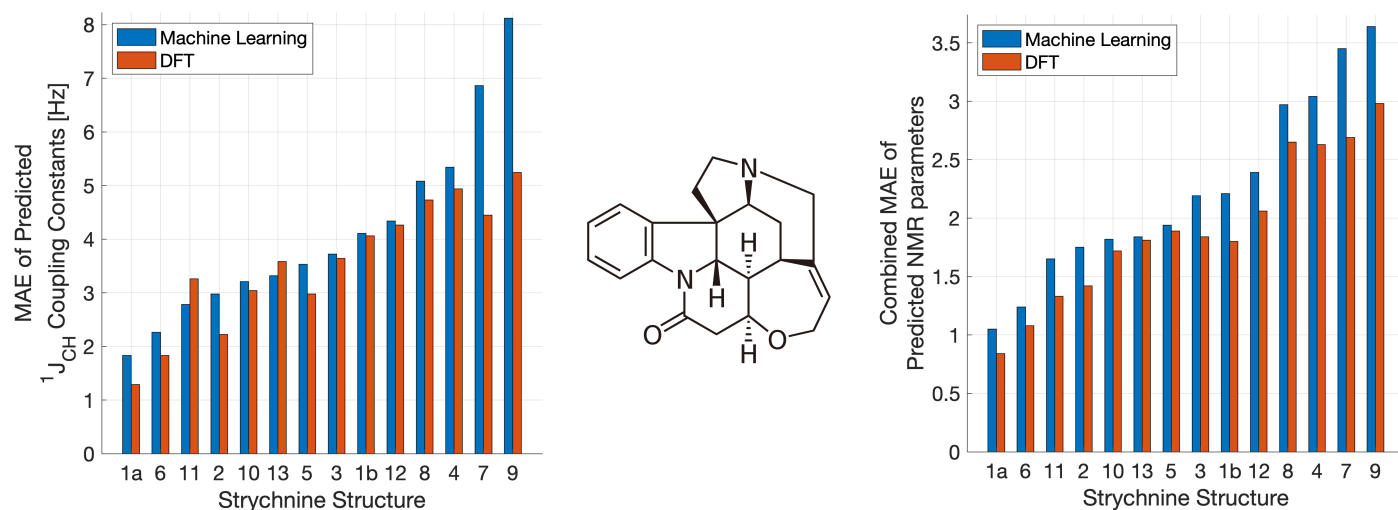


Fig. 5 Errors from comparison of NMR experimental data of the natural product strychnine (centre) to IMPRESSION (blue) and DFT (red) predictions for 13 diastereomers of strychnine, including two conformers for the natural product 1: the lowest energy 1a (>97% populated) and the next lowest energy 1b (<3% populated). The left hand plot shows MAE for $^1J_{CH}$ while the right hand plot shows the geometric mean error for all NMR parameters (δ^1H , $\delta^{13}C$ and $^1J_{CH}$) combined. Variance filters applied to predictions: $\delta^1H = 0.1\text{ppm}$, $\delta^{13}C = 5\text{ppm}$, $^1J_{CH} = 1\text{Hz}$.

tural environments of ^{13}C nuclei in molecules are inherently more complex than 1H given the higher valency and thus more complex bonding environments and geometries, so in future development, larger training datasets focussed on optimising $\delta^{13}C$ predictions will be beneficial.

2.4 3-Dimensional structure discrimination

A demanding test of IMPRESSION is in its ability to predict and discriminate experimental NMR data for stereoisomeric compounds i.e. those that differ only in their 3-dimensional structure, but not connectivity. Even though IMPRESSION has not been explicitly trained to deal with multiple conformers/isomers of any one compound, 3-dimensional variation is implicit within the varied chemical structural space of the adaptively sampled training set. Buevich *et al* recently demonstrated⁵ that DFT prediction of $^1J_{CH}$ values can successfully discriminate the naturally occurring structure 1 of the polycyclic alkaloid strychnine (Figure 5, centre) from 12 other diastereomers (see supplementary information section S5 for the structures) based on comparison with the experimental $^1J_{CH}$ values of the natural product. Pleasingly, the same test conducted with IMPRESSION-predicted $^1J_{CH}$ values (blue bars in Figure 5, left) also correctly identifies the natural product diastereomer 1a as having the smallest error (MAE = 1.87Hz; RMSE = 2.50Hz; MaxE = 6.19Hz). The error for the correct structure is ~30% lower than the diastereomer with the second lowest error 6 (MAE = 2.48Hz; RMSE = 3.38Hz; MaxE = 8.42Hz) and this is very similar to the discrimination offered by $\omega b97xd/6-311g(d,p)$ (red bars in Figure 5). Indeed IMPRESSION could also distinguish between the 3-dimensional structures of 1a, the lowest energy conformer of the natural product (97% population in solution), and 1b which is the second lowest energy conformer (3% population in solution)⁴⁵. So while the absolute accuracy of IMPRESSION for predicting $^1J_{CH}$ values for strychnine (MAE = 1.87Hz) is slightly lower than that obtained from

the DFT method (MAE = 1.31Hz), its discriminating power between structural isomers is nearly the same.

Combining IMPRESSION predictions for $^1J_{CH}$ with 1H and ^{13}C chemical shifts also provides correct identification of the naturally occurring structure, but IMPRESSION and DFT now both see structure 2 as the next best candidate (Figure 5, right). This is due to the experimental δ^1H values having better agreement with the predictions for diastereomer 2 than 1a for DFT and also IMPRESSION. While this is obviously problematic for structure elucidation purposes, it clearly arises because of a deficiency in the DFT prediction of 1H chemical shifts, which is then faithfully reproduced by IMPRESSION. For the individual MAE values across all three parameters see supplementary information section S5.

Similarly, we found that IMPRESSION predictions can be used to correctly assign the diastereotopic protons in strychnine. IMPRESSION and DFT predictions of $^1J_{CH}$ for the diastereotopic protons in strychnine were consistently in line with each other (details can be found in Section S4 of the SI) and for the three methylene groups where there is a significant difference (>2Hz) in experimental $^1J_{CH}$ values both methods correctly assign these protons (Figure S16).

Finally, we validated IMPRESSION chemical shift predictions for natural product structures. We conducted DFT and IMPRESSION predictions on structures from a recent report which suggested structural reassignments for oxirane-containing natural products on the basis of DU8+ DFT calculations⁴⁶. To avoid complications with incorrect DFT prediction of conformer energies leading to poor population averaging of NMR parameters from the constituent conformers, we limited the validation to 'rigid' structures in the report that contained only one dominant conformer after conformational searching. Pleasingly, while our results did not always agree with the DU8+ analysis, IMPRESSION was just as effective as our underlying $\omega b97xd/6-311g(d,p)$ DFT method in discriminating each original and revised chemical structure (see section S3 in the supplementary information for

more details). Once again this confirms that IMPRESSION is capable of making predictions that are of comparable quality to it's underlying DFT method ω b97xd/6-311g(d,p), and thus any improvements in the DFT method used to train IMPRESSION will be subsequently expressed in the quality of IMPRESSION predictions.

3 Conclusions

In summary, this first generation IMPRESSION machine, trained on DFT-computed NMR parameters derived from a set of 3-dimensional structures is capable of reproducing DFT-predicted NMR parameters for a range of experimentally relevant systems with high accuracy but in a fraction of the time. Accurate and generalised prediction of NMR parameters for 3-dimensional applications has not been addressed by previous machine learning systems but the confidence provided by the variance-filtered IMPRESSION results makes this tool essentially as robust for 3-dimensional applications to experimental systems as DFT. At this stage, the two primary sources of error in IMPRESSION predictions of experimental data are errors in the underlying DFT method on which it is trained (of which there can be several^{47–49}) and the range of chemical space covered by the current IMPRESSION training set. We are working to improve both of these factors, as well as extending the predictions to multiple-bond scalar couplings for future generations of IMPRESSION, along with developing a more rigorous statistical treatment of the predicted values taking into account the pre-prediction variance.

Conflicts of interest

There are no conflicts to declare.

Acknowledgements

This work was carried out using the computational facilities of the Advanced Computing Research Centre, University of Bristol - <http://www.bristol.ac.uk/acrc/>. We thank Dr Peter Howe (Syngenta, UK) for useful discussions regarding the experimental $^1J_{\text{CH}}$ dataset used. WG thanks the EPSRC National Productivity Investment Fund (NPIF) for Doctoral Studentship funding. LAB thanks the Alan Turing Institute under the EPSRC grant EP/N510129/1. DRG acknowledges funding from the Royal Society as a University Research Fellow, and also from EPSRC grant EP/M022129/1. AJM thanks EPSRC for funding (EP/M022609/1, CCP-BioSim). LAB and DRG acknowledge support of this work through EPSRC grant EP/P021123/1. We further acknowledge the use of the following software: BayesianOptimization⁵⁰, Open Babel⁵¹, Pybel⁵², NumPy⁵³, OpenMP⁵⁴, F2PY⁵⁵.

Notes and references

- 1 E. Pretsch, T. Clerc, J. Seibl and W. Simon, *Tables of spectral data for structure determination of organic compounds*, Springer Science & Business Media, 2013.
- 2 W. Bremser, *Anal. Chim. Acta*, 1978, **103**, 355–365.
- 3 S. Kuhn and S. R. Johnson, *ACS Omega*, 2019, **4**, 7323–7329.
- 4 J. Aires-de Sousa, M. C. Hemmer and J. Gasteiger, *Anal. Chem.*, 2002, **74**, 80–90.
- 5 A. V. Buevich, J. Saurí, T. Parella, N. De Tommasi, G. Bifulco, R. T. Williamson and G. E. Martin, *Chem. Commun.*, 2019, **55**, 5781–5784.
- 6 J. Meiler, W. Maier, M. Will and R. Meusinger, *J. Mag. Reson.*, 2002, **157**, 242–252.
- 7 C. Haasnoot, F. A. de Leeuw and C. Altona, *Tetrahedron*, 1980, **36**, 2783–2792.
- 8 B. Coxon, *Adv. Carbohydr. Chem. Biochem.*, 2009, **62**, 17–82.
- 9 A. Navarro-Vázquez, *Magn. Reson. Chem.*, 2017, **55**, 29–32.
- 10 M. W. Lodewyk, M. R. Siebert and D. J. Tantillo, *Chem. Rev.*, 2011, **112**, 1839–1862.
- 11 C. Steinmann, L. A. Bratholm, J. M. H. Olsen and J. Kongsted, *J. Chem. Theory Comput.*, 2017, **13**, 525–536.
- 12 A. S. Larsen, L. A. Bratholm, A. S. Christensen, M. Channir and J. H. Jensen, *PeerJ*, 2015, **3**, e1344.
- 13 T. Helgaker, M. Jaszuński and M. Pecul, *Prog. Nucl. Magn. Reson. Spectrosc.*, 2008, **4**, 249–268.
- 14 S. N. Maximoff, J. E. Peralta, V. Barone and G. E. Scuseria, *J. Chem. Theory Comput.*, 2005, **1**, 541–545.
- 15 J. F. San, J. de la Vega García, R. Suardiáz, M. Fernández-Oliva, C. Pérez, R. Crespo-Otero and R. Contreras, *Magn. Reson. Chem.*, 2013, **51**, 775–787.
- 16 N. Grimblat, M. M. Zanardi and A. M. Sarotti, *J. Org. Chem.*, 2015, **80**, 12526–12534.
- 17 V. A. Semenov and L. B. Krivdin, *Magn. Reson. Chem.*, 2019.
- 18 *NMR Prediction Software from ACD/Labs*, https://www.acdlabs.com/products/adh/nmr/nmr_pred/.
- 19 *NMR Prediction Software from Mestrelab*, <https://mestrelab.com/software/mnova/nmr-predict/>.
- 20 A. M. Castillo, A. Bernal, R. Dieden, L. Patiny and J. Wist, *J. Cheminf.*, 2016, **8**, 26.
- 21 A. J. Brandolini, *NMRPredict Modgraph Consultants, Ltd, 1348 Graham Place, Escondido, CA 92129*. <http://www.modgraph-usa.com>, 2006.
- 22 F. M. Paruzzo, A. Hofstetter, F. Musil, S. De, M. Ceriotti and L. Emsley, *Nat. Commun.*, 2018, **9**, 4501.
- 23 C. Venkata, M. J. Forster, P. W. Howe and C. Steinbeck, *PLOS ONE*, 2014, **9**, e111576.
- 24 M. Frisch, G. Trucks, H. Schlegel, G. Scuseria, M. Robb, J. Cheeseman, G. Scalmani, V. Barone, B. Mennucci, G. Petersson and s. S. S. o. S. I. others (for the full reference, *Wallingford, CT*, 2016.
- 25 A. M. Teale, O. B. Lutnæs, T. Helgaker, D. J. Tozer and J. Gauss, *J. Chem. Phys.*, 2013, **138**, 024111.
- 26 C. Adamo and V. Barone, *J. Chem. Phys.*, 1998, **108**, 664–675.
- 27 A. McLean and G. Chandler, *J. Chem. Phys.*, 1980, **72**, 5639–5648.
- 28 R. Krishnan, J. S. Binkley, R. Seeger and J. A. Pople, *J. Chem. Phys.*, 1980, **72**, 650–654.
- 29 J.-D. Chai and M. Head-Gordon, *J. Chem. Phys.*, 2008, **128**, 084106.
- 30 W. Deng, J. R. Cheeseman and M. J. Frisch, *J. Chem. Theory Comput.*, 2006, **2**, 1028–1037.

- 31 P. B. Wilson, M. Grootveld and S. C. L. Kamerlin, *Magn. Reson. Chem.*, 2019.
- 32 R. Laskowski, P. Blaha and F. Tran, *CHESHIRE Chemical Shift Repository*, 2019 (accessed October 2nd, 2019).
- 33 H. S. Seung, M. Oppen and H. Sompolinsky, Proc. 5th Ann. Work. Comp. Learn. Theory, New York, NY, USA, 1992, pp. 287–294.
- 34 M. Gastegger, J. Behler and P. Marquetand, *Chem. Sci.*, 2017, **8**, 6924–6935.
- 35 J. S. Smith, B. Nebgen, N. Lubbers, O. Isayev and A. E. Roitberg, *J. Chem. Phys.*, 2018, **148**, 241733.
- 36 C. R. Groom, I. J. Bruno, M. P. Lightfoot and S. C. Ward, *Acta Crystallogr. B*, 2016, **72**, 171–179.
- 37 C. Saunders, A. Gammerman and V. Vovk, 1998.
- 38 Y. Binev and J. Aires-de Sousa, *J. Chem. Inf. Comput. Sci.*, 2004, **44**, 940–945.
- 39 Y. Binev, M. M. Marques and J. Aires-de Sousa, *J. Chem. Inf. Model.*, 2007, **47**, 2089–2097.
- 40 M. Rupp, R. Ramakrishnan and O. A. Von Lilienfeld, *J. Phys. Chem. Lett.*, 2015, **6**, 3309–3313.
- 41 B. Huang and O. A. von Lilienfeld, *arXiv preprint arXiv:1707.04146*, 2017.
- 42 F. A. Faber, A. S. Christensen, B. Huang and O. A. von Lilienfeld, *J. Chem. Phys.*, 2018, **148**, 241717.
- 43 A. S. Christensen, L. A. Bratholm, S. Amabilino, J. C. Krohmann, F. A. Faber, B. Huang, A. Tkatchenko, K. R. MÅijller and O. A. von Lilienfeld, *QML: A Python Toolkit for Quantum Machine Learning*, 2019, <https://github.com/qmlcode/qml>.
- 44 S. G. Smith and J. M. Goodman, *J. Am. Chem. Soc.*, 2010, **132**, 12946–12959.
- 45 C. P. Butts, C. R. Jones and J. N. Harvey, *Chem. Commun.*, 2011, **47**, 1193–1195.
- 46 A. G. Kutateladze, D. M. Kuznetsov, A. A. Beloglazkina and T. Holt, *J. Org. Chem.*, 2018, **83**, 8341–8352.
- 47 M. A. Iron, *J. Chem. Theory Comp.*, 2017, **13**, 5798–5819.
- 48 A. Bagno, F. Rastrelli and G. Saielli, *Chem.: Eur. J.*, 2006, **12**, 5514–5525.
- 49 R. Laskowski, P. Blaha and F. Tran, *Physical Review B*, 2013, **87**, 195130.
- 50 F. Nogueira, *A Python implementation of global optimization with gaussian processes*, 2019, <https://github.com/fmfn/BayesianOptimization>.
- 51 N. M. O’Boyle, M. Banck, C. A. James, C. Morley, T. Vandermeersch and G. R. Hutchison, *J. Cheminf.*, 2011, **3**, 33.
- 52 N. M. O’Boyle, C. Morley and G. R. Hutchison, *Chem. Cent. J.*, 2008, **2**, 5.
- 53 T. E. Oliphant, *A guide to NumPy*, Trelgol Publishing USA, 2006, vol. 1.
- 54 L. Dagum and R. Menon, *Comput. Sci. Eng.*, 1998, 46–55.
- 55 P. Peterson, *Int. J. Comput. Sci. Eng.*, 2009, **4**, 296–305.

Supplementary Information for IMPRESSION - Prediction of NMR Parameters using Machine Learning with near-DFT accuracy

Will Gerrard, Lars Andersen Bratholm, Martin Packer, Adrian Mulholland, David Glowacki, Craig Butts

Contents

S1 Methods	2
S1.1 Kernel ridge regression	2
S1.2 Training and test data	2
S1.3 Correction of DFT NMR parameter predictions for comparison to experiment	3
S1.4 Adaptive sampling	3
S1.5 Hyper-parameter optimisation	3
S2 IMPRESSION performance using Molecular Mechanics geometries	4
S2.1 DFT trained model	4
S2.2 MMFF94 trained model	5
S2.3 Computational timings	6
S3 Structure revision examples	7
S3.1 Geometric mean for diastereomer discrimination	7
S3.2 Crithmifolide	7
S3.3 Caespitenone	8
S3.4 Secoafricane	9
S3.5 Grandilobalide B	10
S3.6 Toluene dioxide	11
S4 Diastereotopic proton assignment in Strychnine	12
S5 Strychnine diastereomers	14
S6 Large errors	18
S6.1 ^1H chemical shifts	18
S6.2 ^{13}C chemical shifts	19
S6.3 $^1J_{\text{CH}}$ coupling constant	20
S7 Gaussian input files	21
S8 CSD structures	22
S9 Full Gaussian reference	27

S1 Methods

S1.1 Kernel ridge regression

Kernel Ridge Regression[?] (KRR) provides a systematic way to map geometric features of a chemical environment (i.e. the chemical identity and geometry of atoms in the environment surrounding atoms of interest) to a target observable (in this case scalar coupling constants or chemical shifts), effectively interpolating between known data points. The observable of interest (y_i) for a given environment (\mathbf{E}_i) is estimated as a linear combination of it's similarity to the environments (\mathbf{E}_j), for which the corresponding observable is known:

$$y_i^{\text{pred}} = \sum_j^N \alpha_j k(\mathbf{E}_i, \mathbf{E}_j), \quad (1)$$

Here N is the number of chemical environments in the training data set and k is a kernel function that computes the similarity between two environments. The kernel function typically takes a value of 1 for identical environments and approaches asymptotically 0 when environments become increasingly different. The regression parameters α are regression coefficients that can be fitted to the training data by regularized least-squares optimization:

$$\underset{\alpha}{\text{minimise}} \sum_i^N \left(y_i^{\text{exp}} - y_i^{\text{pred}} \right)^2 + \lambda \sum_i^N \alpha_i^2, \quad (2)$$

where y_i^{pred} is given by equation (1). λ controls the strength of the l_2 -regularization, which is a penalty term to the loss function that favours the regression coefficients to be more uniform and to take smaller values. This effectively reduces overfitting and if properly tuned can improve transferability to new chemical environments.

Several functional forms of the kernel similarity measure has been proposed in recent years. In this work we compare three different kernel functions. The atomic Coulomb Matrix[?] was one of the early successful vector representations of the chemical environment around an atom and includes two-body interactions (distances) between a given atom and all atoms within a specified cutoff radius. The Atomic Spectral London Axilrod-Teller-Muto[?] (aSLATM) representation is a separate approach that also includes three-body interactions (angles). Both representations generate a vector (\mathbf{x}) per environment, where the kernel similarity can computed with a laplacian kernel:

$$k(\mathbf{E}_i, \mathbf{E}_j) = \exp \left(- \frac{\|\mathbf{x}_i - \mathbf{x}_j\|_1}{\sigma} \right), \quad (3)$$

where the kernel width σ determines how quickly the similarity measure converges towards 0.

FCHL[?] (acronym derived from the authors surnames) also includes three-body terms, but generates the kernel similarity directly, rather than through an intermediate vector representation step.

Since the above kernel similarity measure indicates how similar the chemical environment around two *atoms* are, we chose to use the product of the kernel similarity between the two hydrogens and the two carbons to represent $^1\text{J}_{\text{CH}}$ environments:

$$k(\mathbf{E}_i^{\text{CH}}, \mathbf{E}_j^{\text{CH}}) = k(\mathbf{E}_i^{\text{H}}, \mathbf{E}_j^{\text{H}}) k(\mathbf{E}_i^{\text{C}}, \mathbf{E}_j^{\text{C}}), \quad (4)$$

where \mathbf{E}_i^{CH} is the joint set of chemical environments around the hydrogen and carbon atom involved in the scalar coupling. Alternatively just the kernel similarity between hydrogen atoms could be used, but we found an improvement in performance by also including the carbon similarity.

All representations and kernels as well as optimisation of the regression parameters were performed with the QML python library[?].

S1.2 Training and test data

The KRR machine was trained using 17,222 coupling environments from 882 chemical structures selected by adaptive sampling (active learning)^{???} from the Cambridge structural database (filtering first for structures that contain only C, H, N, O and F elements, see section S1.4 for details) then optimising the structures and calculating the DFT NMR parameters (see next paragraph for details). The test set contained an independent set of 7832 environments from 410 chemical structures from the randomly selected CSD-500 test set reported by Emsley et al[?]. All DFT calculations were carried out using the Gaussian09 Rev. D software package[?] (See section S7 for example input files). The 3-dimensional chemical structures were each optimised with *mPW1PW91*[?]/6-311g(d,p)^{??} using tight optimisation criteria and ultra-fine integral grids were used to minimise molecular orientation affecting geometries and energies (see reference[?] and references therein for a discussion of this) and the resulting optimised structures were used to compute NMR parameters with *wb97xd*[?]/6-311g(d,p). The NMR computations used gauge independent atomic orbitals and were conducted with an uncontracted basis set for coupling calculations[?], called with the 'mixed' option within the Gaussian09 software. The scalar coupling values obtained from the calculations included all terms calculated: Fermi contact, spin-dipolar, paramagnetic spin-orbit and diamagnetic spin orbit terms are all included in the total nuclear spin-spin coupling produced in the output files. Some DFT structure optimisations failed to converge to an energy minima and these were excluded from the final datasets.

S1.3 Correction of DFT NMR parameter predictions for comparison to experiment

The DFT calculated magnetic shielding tensors were converted to chemical shifts using a linear scaling method and reference compounds reported by Tantillo *et al.*². The results of this linear scaling are shown in figure S1.

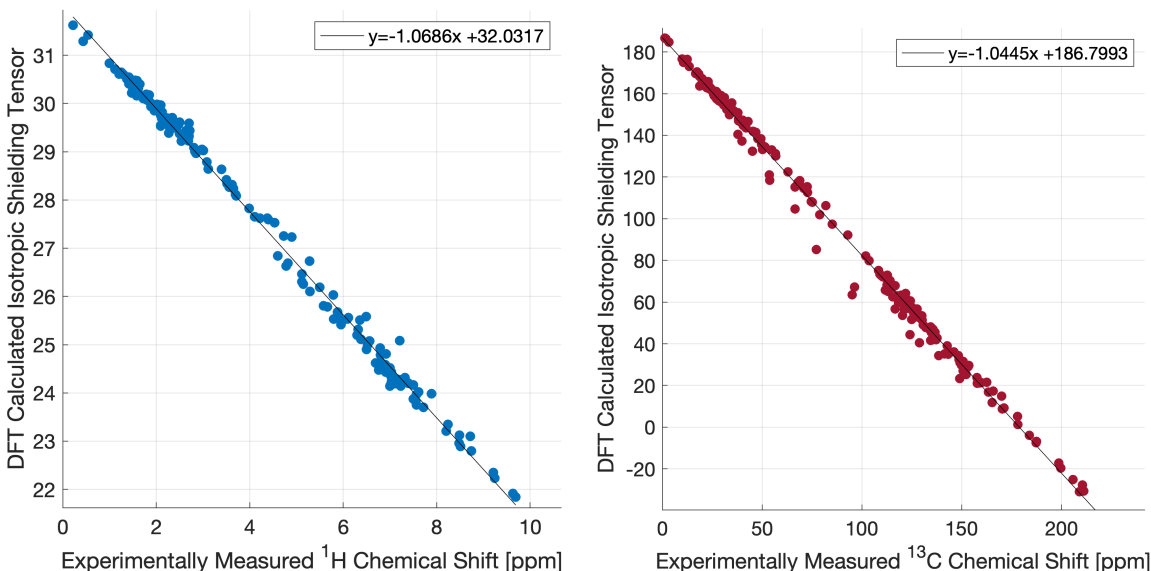


Figure S1 Calculation of tantillo regression scaling factors for a) $\delta^1\text{H}$ and b) $\delta^{13}\text{C}$

For the $^1J_{\text{CH}}$ data used in this work, a clear linear offset was found upon comparison of the DFT values to experimentally measured data. As a result, the offset (10.91Hz) was applied to the DFT values in both the training and test datasets.

S1.4 Adaptive sampling

The training set was obtained via an adaptive sampling approach. An initial set of 100 structures were chosen at random from the CSD-500 test set already obtained from the work by Emsley *et al.*². 5 subsets of 80 structures each were then used to train separate models to predict $^1J_{\text{CH}}$ coupling constants, ^1H and ^{13}C chemical shifts for all organic structures in the Cambridge Structural Database containing only H/C/N/O/F atoms. The variance in the predictions of the five models (pre-prediction variance) is a measure of how confident one can be in a given prediction. 300 structures containing the environments with the highest variance were selected to be added to the training set (100 each based on the $^1J_{\text{CH}}$, ^1H and ^{13}C variance). Structure optimizations and NMR computations were performed for these to build the training set. The initial random set of 100 structures was discarded after the first round, and the process was repeated four times. Some structures failed to optimise in each round and were discarded leading to a training set consisting of 882 structures.

S1.5 Hyper-parameter optimisation

The following hyper-parameters were optimized for the machine learning procedure: the cutoff radius, the kernel width and the l2-regularisation factor. The optimal combination of these three variables was found through a cross-validated gaussian-process led search using the python module BayesianOptimization⁷. The optimal parameters were determined as those with the lowest average mean absolute deviation across a five-fold cross-validation using the training set environments.

S2 IMPRESSION performance using Molecular Mechanics geometries

Whilst the focus of this work is to develop a machine learning method to replace the DFT calculation of NMR parameters, the geometry optimisation used in preparing the structures in all datasets still accounts for 26% of the total CPU time. The effect of replacing the DFT geometry optimisation step with a molecular mechanics based optimisation was investigated through two methods.

S2.1 DFT trained model

Firstly, the existing models (trained using DFT optimised geometries) were used to make predictions on structures optimised through the MMFF94 forcefield². The result was a decrease in accuracy of all three models but especially so for $^1J_{CH}$ and $\delta^{13}C$. The error distributions in figure S2 show a reduction in the quality of the predictions on all three parameters.

	MAE	RMSE	MaxE	Variance Cutoff	Envs removed
δ^1H	0.26ppm	0.38ppm	5.55ppm	0.1ppm	1
$\delta^{13}C$	3.30ppm	4.63ppm	37.42ppm	5ppm	949
$^1J_{CH}$	2.30Hz	3.00Hz	20.44Hz	1Hz	5009

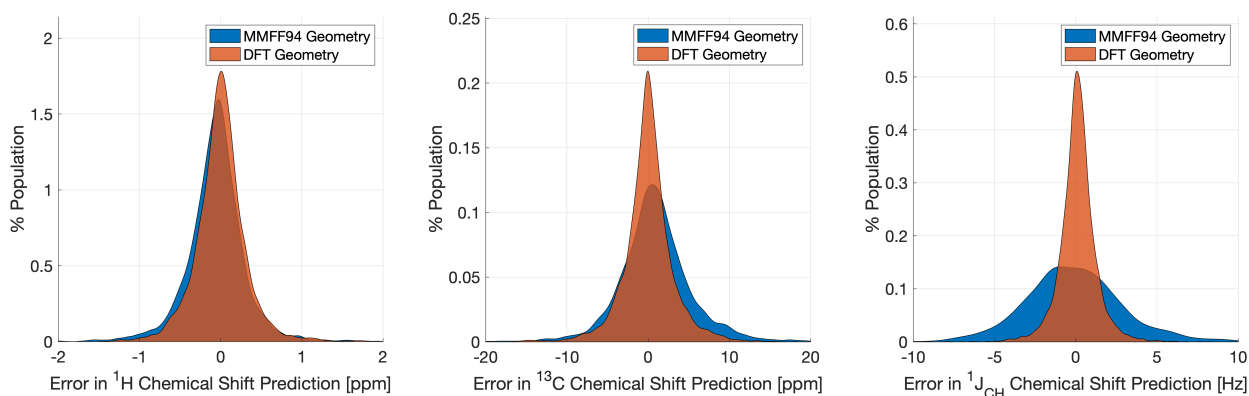


Figure S2 Error distributions for IMPRESSION predictions of molecular mechanics structures, using IMPRESSION models trained using DFT geometries. Variance filters applied: $\delta^1H = 0.1\text{ppm}$, $\delta^{13}C = 5\text{ppm}$, $^1J_{CH} = 1\text{Hz}$.

S2.2 MMFF94 trained model

Additionally, new models were trained based on molecular mechanics optimised training structures. The entire set of training and testing structures were reoptimised using the MMFF94⁷ forcefield. These structures were associated with the previously calculated DFT NMR parameters and used to train and test new models. The model hyper-parameters were optimised using the same method as the DFT trained models and achieved an accuracy which was up to 50% worse than the models trained using DFT optimised structures.

	MAE	RMSE	MaxE	Variance Cutoff	Envs removed
$\delta^1\text{H}$	0.28ppm	0.40ppm	5.20ppm	0.1ppm	3
$\delta^{13}\text{C}$	2.31ppm	3.48ppm	39.92ppm	5ppm	952
$^1J_{\text{CH}}$	1.19Hz	1.75Hz	20.40Hz	5Hz	143

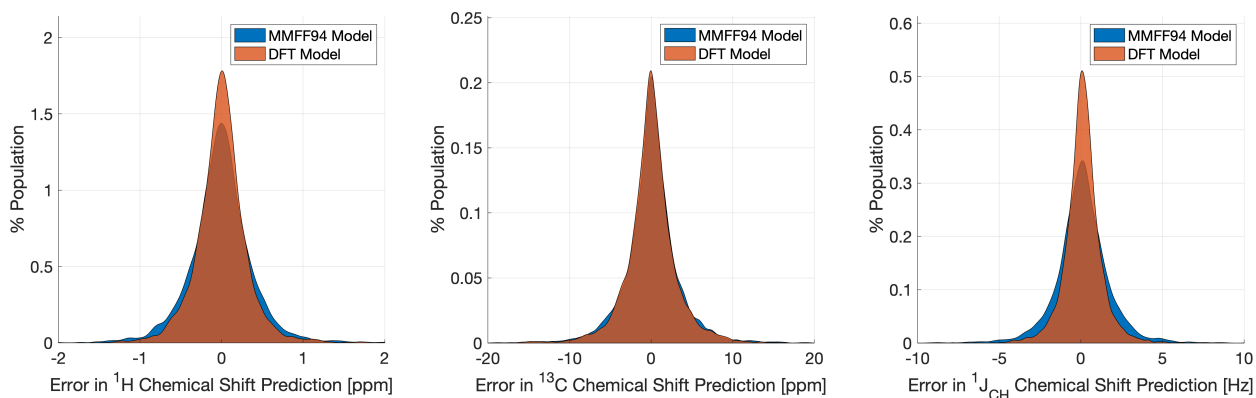


Figure S3 Error distributions for models trained using MMFF94 geometries predicting on structures with MMFF94 geometries, compared to the original DFT models from the main text. Variance filters applied: $\delta^1\text{H} = 0.1\text{ppm}$, $\delta^{13}\text{C} = 5\text{ppm}$, $^1J_{\text{CH}} = 1\text{Hz}$.

S2.3 Computational timings

To highlight the value of replacing the NMR calculation with a machine learning solution, the distributions of CPU cost for all calculations in producing the training set are included here in figure S4. The 'mixed' option which uses an uncontracted basis set for calculating the fermi contact term is only relevant for coupling calculations so this has been removed from figure S4b. The mean CPU time for an optimisation was 15 hours across all 882 structures, whilst the mean CPU time for a DFT NMR calculation was 42 hours (or 22 hours without mixed). The use of a machine learning model to replace the NMR calculation therefore represents a significant time saving.

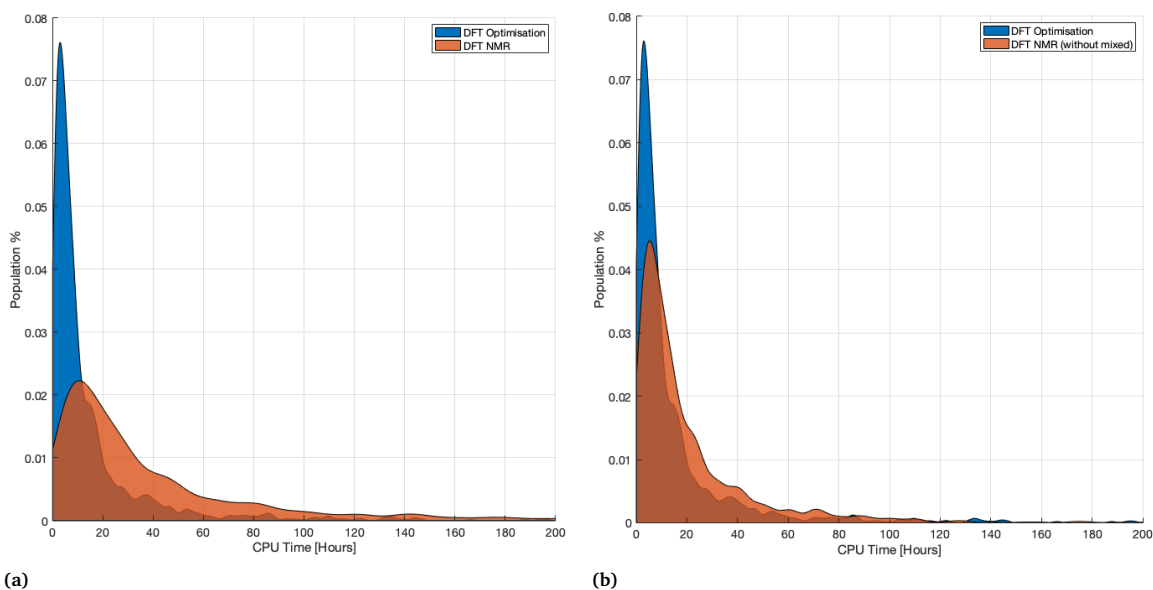


Figure S4 Distribution of CPU time for DFT calculations on the training dataset. Mean time for optimisation = 15 Hours. a) with mixed option: Mean time for NMR calculation = 42 Hours. b) without mixed option: Mean time for NMR calculation = 22 Hours.

S3 Structure revision examples

To further demonstrate the applicability of the IMPRESSION predictions to structural elucidation problems, 5 examples of proposed natural product structure revisions from the literature were investigated². No $^1J_{\text{CH}}$ values were reported for these compounds, so we can only make comparisons using the chemical shift models.

For the 5 compounds, Cartesian coordinates for the original and revised structures were obtained from the literature along with the experimental $\delta^1\text{H}$ and $\delta^{13}\text{C}$ assignments. The Cartesian coordinates were optimised, NMR parameters were computed and IMPRESSION predictions were made for each structure. The mean absolute error between the IMPRESSION predictions and experiment were compared to the corresponding MAE between the DFT calculations and the experimental values. Variance cutoffs of 1Hz, 0.1ppm, and 5ppm were used for $^1J_{\text{CH}}$, $\delta^1\text{H}$, and $\delta^{13}\text{C}$ respectively.

S3.1 Geometric mean for diastereomer discrimination

As we combine different types of data to gather evidence for a given diastereomer, we take the geometric mean of mean absolute errors for each of the parameters:

$$\text{MAE}_{\text{combined}} = \sqrt[3]{\text{MAE}_{^1J_{\text{CH}}} \text{MAE}_{\delta^1\text{H}} \text{MAE}_{\delta^{13}\text{C}}} \quad (5)$$

or in the case where $^1J_{\text{CH}}$ values are not available:

$$\text{MAE}_{\text{combined}} = \sqrt[2]{\text{MAE}_{\delta^1\text{H}} \text{MAE}_{\delta^{13}\text{C}}} \quad (6)$$

S3.2 Crithmifolide

Comparing the results from our DFT method to that used in the original work, the predictions for the ^1H chemical shifts do not show the same improvement in accuracy between the original and revised structures. In the original work an improvement of 0.08ppm RMSE was reported, whereas comparisons using our DFT method found an increase in MAE of 0.03ppm (and RMSE of 0.01ppm). Pleasingly the IMPRESSION results mirror this discrepancy and match the DFT method on which the model was trained.

The ^{13}C chemical shift results from our DFT method agree with the literature, showing an improvement in fit from the original to the revised structure. The indecisive results from the geometric mean comparison reflect this discrepancy between the two chemical shift comparisons.

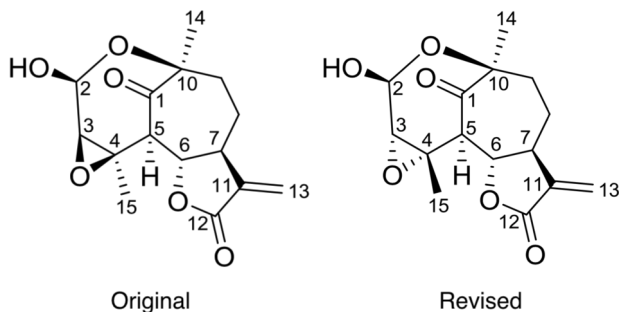


Figure S5 Original and revised structures for Crithmifolide.

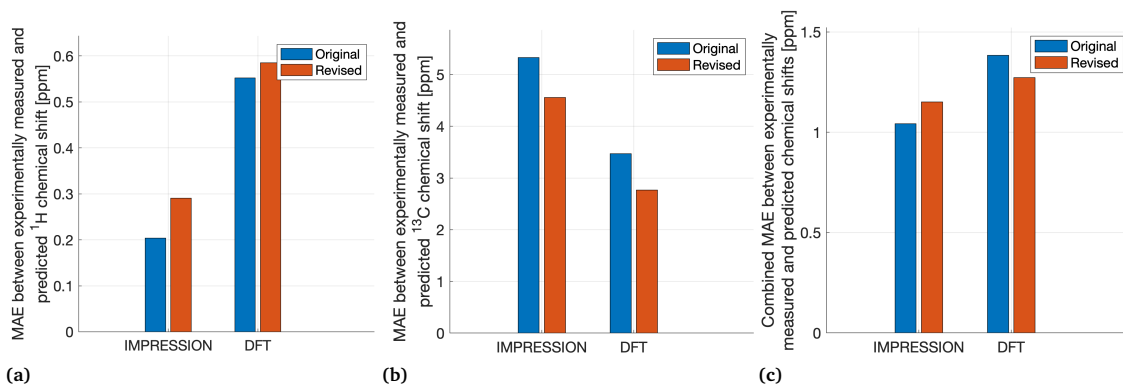


Figure S6 Change in the fit between prediction and experiment for both DFT and IMPRESSION for Crithmifolide. a) $\delta^1\text{H}$. b) $\delta^{13}\text{C}$. c) Geometric mean across both parameters.

S3.3 Caespitenone

The results for Caespitenone show good agreement between IMPRESSION, our DFT method, and the previously published results. Large deviations ($>5\text{ppm}$) were reported in the ^{13}C chemical shift results, and the DFT method used in this work reproduces this. The IMPRESSION predictions show the same change in the fit to experiment.

The methods used in this work also showed a significant improvement in fit for the ^1H chemical shifts, resulting in a reduction in error of over 50% for both our DFT method and IMPRESSION.

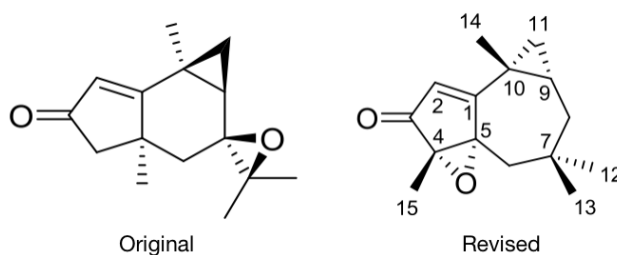


Figure S7 Original and revised structures for Caespitenone

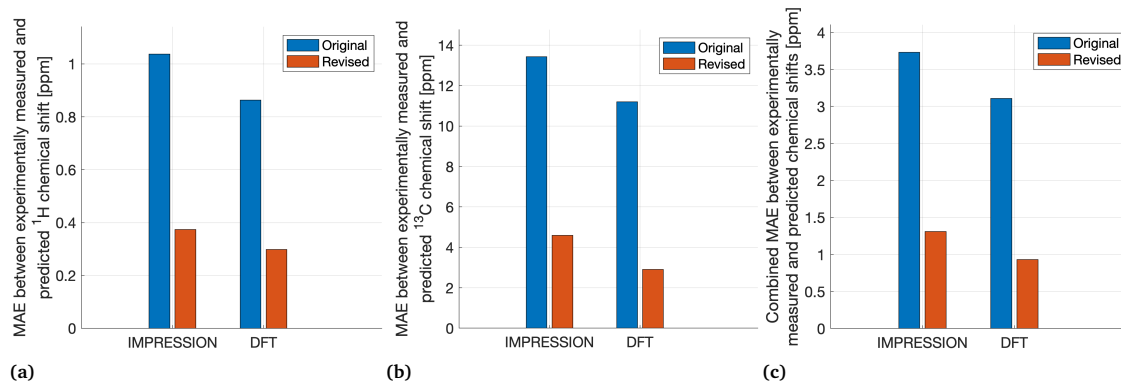


Figure S8 Change in the fit between prediction and experiment for both DFT and IMPRESSION for Caespitenone. a) $\delta^1\text{H}$. b) $\delta^{13}\text{C}$. c) Geometric mean across both parameters.

S3.4 Secoafricane

The reported values in the original work show a significant improvement in fit between experiment and calculation for both ^1H and ^{13}C chemical shifts. The results from our DFT method show a smaller but still significant improvement in fit for both parameters, and IMPRESSION mimics these results, but with a smaller change in MAE for the ^{13}C comparison.

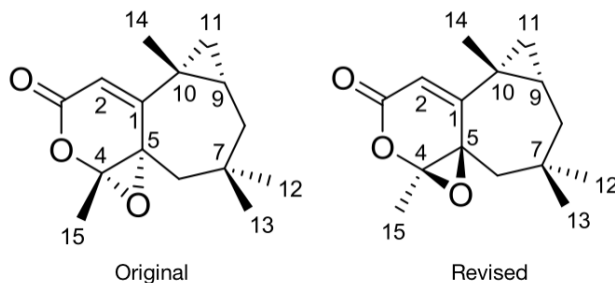


Figure S9 Original and revised structures for Secoafricane.

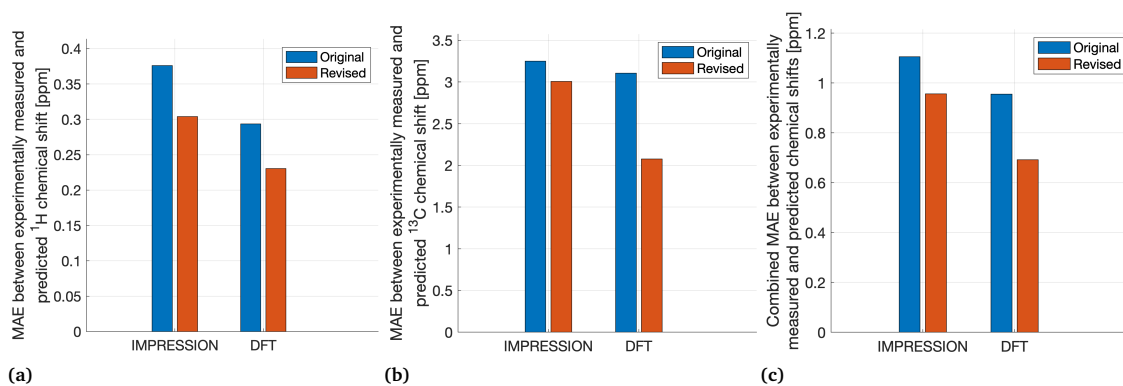


Figure S10 Change in the fit between prediction and experiment for both DFT and IMPRESSION for Secoafricane. a) $\delta^1\text{H}$. b) $\delta^{13}\text{C}$. c) Geometric mean across both parameters.

S3.5 Grandilobalide B

The literature results for Grandilobalide B show a large improvement in fit for ^{13}C chemical shift, which is not reproduced in our results. The results for ^1H chemical shifts are reproduced, in the literature a small decrease in the fit to experiment from 0.27ppm RMSE to 0.33ppm RMSE is reported. Both IMPRESSION and our DFT method show a small but significant reduction in fit for the revised structure.

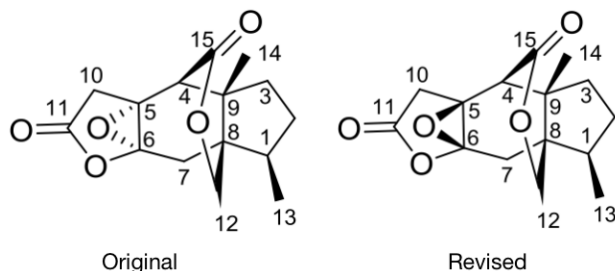


Figure S11 Original and revised structures for Grandilobalide B.

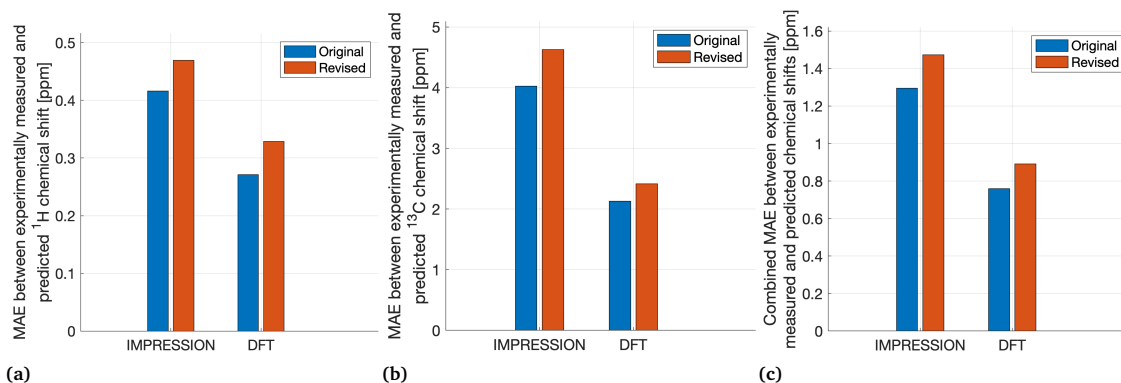


Figure S12 Change in the fit between prediction and experiment for both DFT and IMPRESSION for Grandilobalide B. a) $\delta^1\text{H}$. b) $\delta^{13}\text{C}$. c) Geometric mean across both parameters.

S3.6 Toluene dioxide

In the original work, a large improvement in the fit to experiment for both ^{13}C and ^1H chemical shift was reported. The results from our DFT method were inconclusive for both parameters in this case. Pleasingly IMPRESSION mimics the DFT results, irrespective of the DFT methods fit to the reported results.

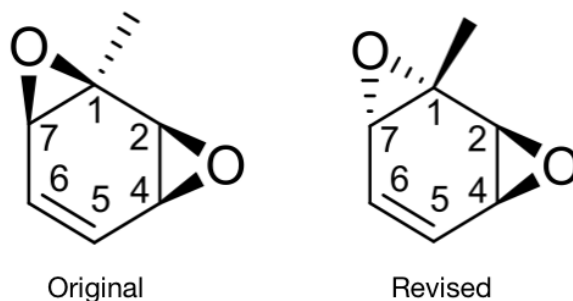


Figure S13 Original and revised structures for Toluene Dioxide

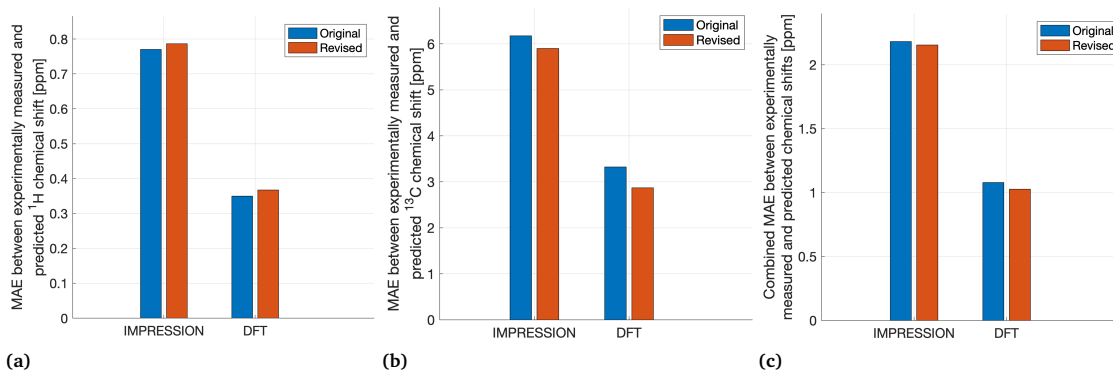


Figure S14 Change in the fit between prediction and experiment for both DFT and IMPRESSION for Toluene Dioxide. a) $\delta^1\text{H}$. b) $\delta^{13}\text{C}$. c) Geometric mean across both parameters.

S4 Diastereotopic proton assignment in Strychnine

Further analysis was performed to see if the $^1J_{CH}$ IMPRESSION predictions could be used to assign the diastereotopic protons in strychnine. The $^1J_{CH}$ values for the 3 sets of diastereotopic protons for diastereomer 1 were compared across the three data sources: IMPRESSION predictions, DFT calculations and experimental measurements.

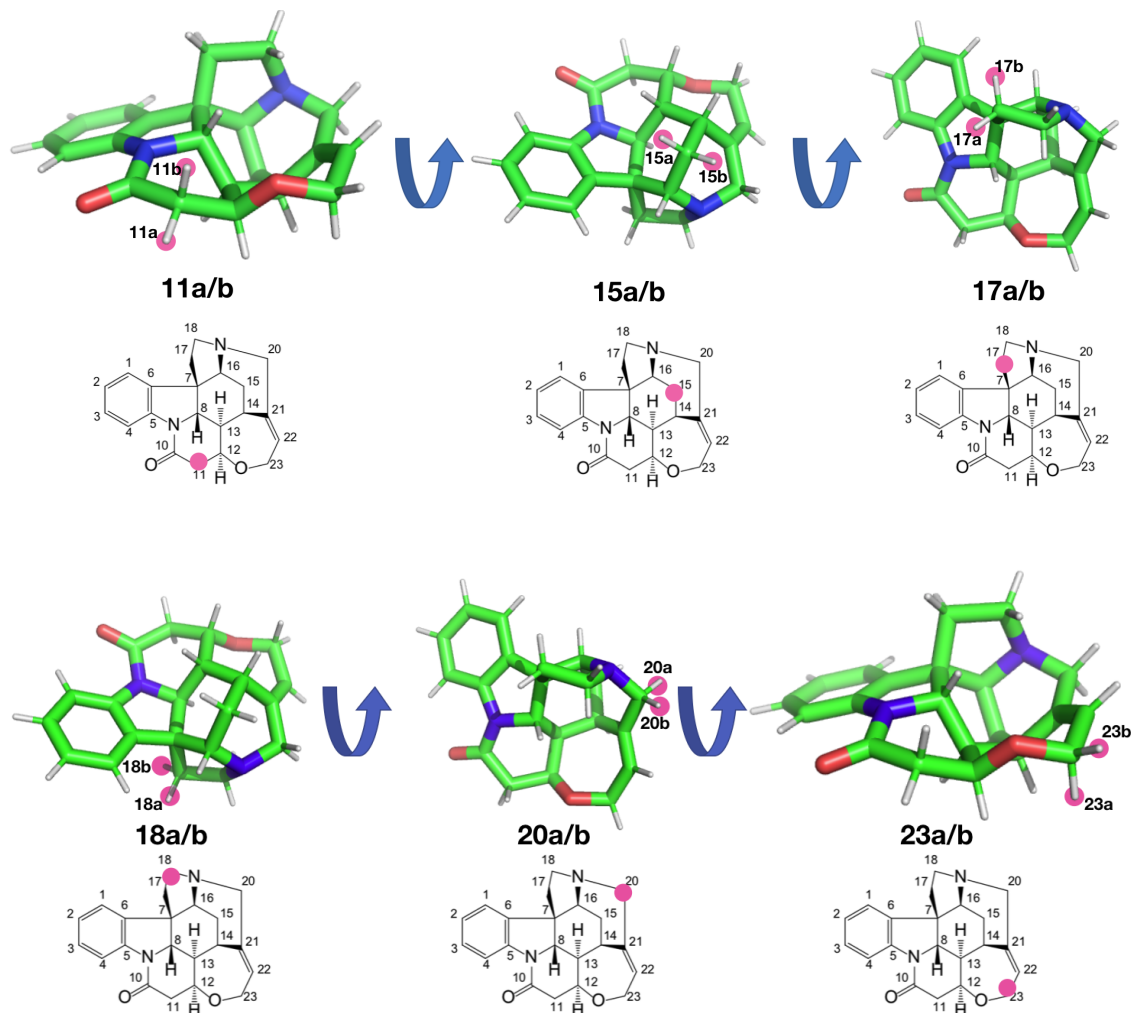


Figure S15 Identification of the diastereotopic protons in Strychnine

The results show that in cases where there is the three methylenes were there is any significant ($>2\text{Hz}$) difference in the experimental $^1J_{CH}$ values (figures S16a, S16b, S16c) the DFT method and IMPRESSION predictions can distinguish between the diastereotopic protons and correctly assign them. Where the difference in experimental values is small (Figure S17, both DFT and IMPRESSION are not reliable for assignment).

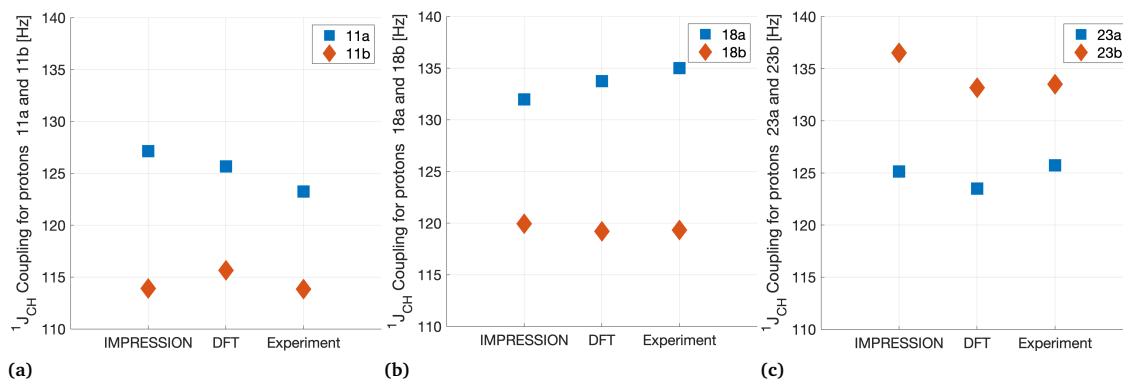


Figure S16 Comparison of $^1J_{CH}$ values across all data sources for diastereotopic protons showing significant experimental difference. a) 11a/b. b) 18a/b. c) 23a/b.

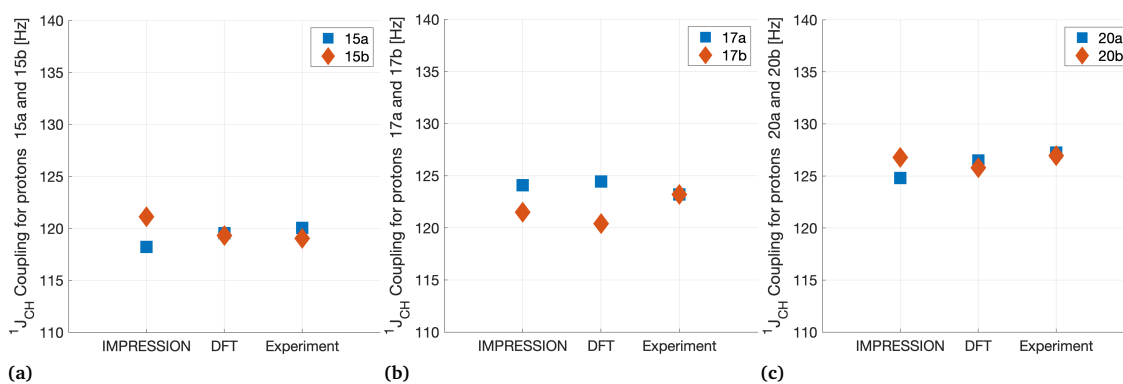


Figure S17 Comparison of $^1J_{CH}$ values across all data sources for diastereotopic protons showing small experimental difference. a) 15a/b. b) 17a/b. c) 20a/b.

S5 Strychnine diastereomers

MAE values for each of the parameters across each of the 14 strychnine structures compared to experiment:

Structure	Parameters	MAE [IMP-EXP]	MAE [DFT-EXP]
1a	$\delta^1\text{H}$	0.28ppm	0.25ppm
1b	$\delta^1\text{H}$	0.73ppm	0.56ppm
2	$\delta^1\text{H}$	0.23ppm	0.19ppm
3	$\delta^1\text{H}$	0.37ppm	0.35ppm
4	$\delta^1\text{H}$	0.69ppm	0.52ppm
5	$\delta^1\text{H}$	0.44ppm	0.32ppm
6	$\delta^1\text{H}$	0.42ppm	0.35ppm
7	$\delta^1\text{H}$	0.77ppm	0.54ppm
8	$\delta^1\text{H}$	0.71ppm	0.53ppm
9	$\delta^1\text{H}$	0.70ppm	0.66ppm
10	$\delta^1\text{H}$	0.48ppm	0.49ppm
11	$\delta^1\text{H}$	0.55ppm	0.49ppm
12	$\delta^1\text{H}$	0.57ppm	0.36ppm
13	$\delta^1\text{H}$	0.73ppm	0.45ppm

Structure	Parameters	MAE [IMP-EXP]	MAE [DFT-EXP]
1a	$\delta^{13}\text{C}$	2.26	1.87
1b	$\delta^{13}\text{C}$	4.54	3.84
2	$\delta^{13}\text{C}$	2.75	2.94
3	$\delta^{13}\text{C}$	4.34	3.98
4	$\delta^{13}\text{C}$	7.69	7.11
5	$\delta^{13}\text{C}$	3.44	2.99
6	$\delta^{13}\text{C}$	4.77	3.63
7	$\delta^{13}\text{C}$	7.77	8.09
8	$\delta^{13}\text{C}$	7.21	7.41
9	$\delta^{13}\text{C}$	8.47	7.73
10	$\delta^{13}\text{C}$	3.98	3.98
11	$\delta^{13}\text{C}$	4.80	4.22
12	$\delta^{13}\text{C}$	5.05	3.79
13	$\delta^{13}\text{C}$	5.53	3.84

Structure	Parameters	MAE [IMP-EXP]	MAE [DFT-EXP]
1a	$^1J_{CH}$	1.83Hz	1.29Hz
1b	$^1J_{CH}$	4.11Hz	4.06Hz
2	$^1J_{CH}$	2.98Hz	2.22Hz
3	$^1J_{CH}$	3.72Hz	3.64Hz
4	$^1J_{CH}$	5.34Hz	4.94Hz
5	$^1J_{CH}$	3.53Hz	2.98Hz
6	$^1J_{CH}$	2.26Hz	1.83Hz
7	$^1J_{CH}$	6.86Hz	4.45Hz
8	$^1J_{CH}$	5.08Hz	4.73Hz
9	$^1J_{CH}$	8.12Hz	5.24Hz
10	$^1J_{CH}$	3.21Hz	3.04Hz
11	$^1J_{CH}$	2.78Hz	3.26Hz
12	$^1J_{CH}$	4.34Hz	4.26Hz
13	$^1J_{CH}$	3.32Hz	3.58Hz

Structure	Parameters	MAE [IMP-EXP]	MAE [DFT-EXP]
1a	$\delta^1H + \delta^{13}C$	0.80ppm	0.68ppm
1b	$\delta^1H + \delta^{13}C$	1.83ppm	1.47ppm
2	$\delta^1H + \delta^{13}C$	0.80ppm	0.75ppm
3	$\delta^1H + \delta^{13}C$	1.27ppm	1.18ppm
4	$\delta^1H + \delta^{13}C$	2.30ppm	1.92ppm
5	$\delta^1H + \delta^{13}C$	1.24ppm	0.98ppm
6	$\delta^1H + \delta^{13}C$	1.41ppm	1.13ppm
7	$\delta^1H + \delta^{13}C$	2.45ppm	2.09ppm
8	$\delta^1H + \delta^{13}C$	2.27ppm	1.99ppm
9	$\delta^1H + \delta^{13}C$	2.43ppm	2.25ppm
10	$\delta^1H + \delta^{13}C$	1.39ppm	1.40ppm
11	$\delta^1H + \delta^{13}C$	1.62ppm	1.43ppm
12	$\delta^1H + \delta^{13}C$	1.58ppm	1.17ppm
13	$\delta^1H + \delta^{13}C$	1.78ppm	1.32ppm

Structure	Parameters	MAE [IMP-EXP]	MAE [DFT-EXP]
1a	$\delta^1\text{H} + \delta^{13}\text{C} + {}^1J_{\text{CH}}$	1.05	0.84
1b	$\delta^1\text{H} + \delta^{13}\text{C} + {}^1J_{\text{CH}}$	2.39	2.06
2	$\delta^1\text{H} + \delta^{13}\text{C} + {}^1J_{\text{CH}}$	1.24	1.08
3	$\delta^1\text{H} + \delta^{13}\text{C} + {}^1J_{\text{CH}}$	1.82	1.72
4	$\delta^1\text{H} + \delta^{13}\text{C} + {}^1J_{\text{CH}}$	3.04	2.63
5	$\delta^1\text{H} + \delta^{13}\text{C} + {}^1J_{\text{CH}}$	1.75	1.42
6	$\delta^1\text{H} + \delta^{13}\text{C} + {}^1J_{\text{CH}}$	1.65	1.33
7	$\delta^1\text{H} + \delta^{13}\text{C} + {}^1J_{\text{CH}}$	3.45	2.69
8	$\delta^1\text{H} + \delta^{13}\text{C} + {}^1J_{\text{CH}}$	2.97	2.65
9	$\delta^1\text{H} + \delta^{13}\text{C} + {}^1J_{\text{CH}}$	3.64	2.98
10	$\delta^1\text{H} + \delta^{13}\text{C} + {}^1J_{\text{CH}}$	1.84	1.81
11	$\delta^1\text{H} + \delta^{13}\text{C} + {}^1J_{\text{CH}}$	1.94	1.89
12	$\delta^1\text{H} + \delta^{13}\text{C} + {}^1J_{\text{CH}}$	2.21	1.80
13	$\delta^1\text{H} + \delta^{13}\text{C} + {}^1J_{\text{CH}}$	2.19	1.84

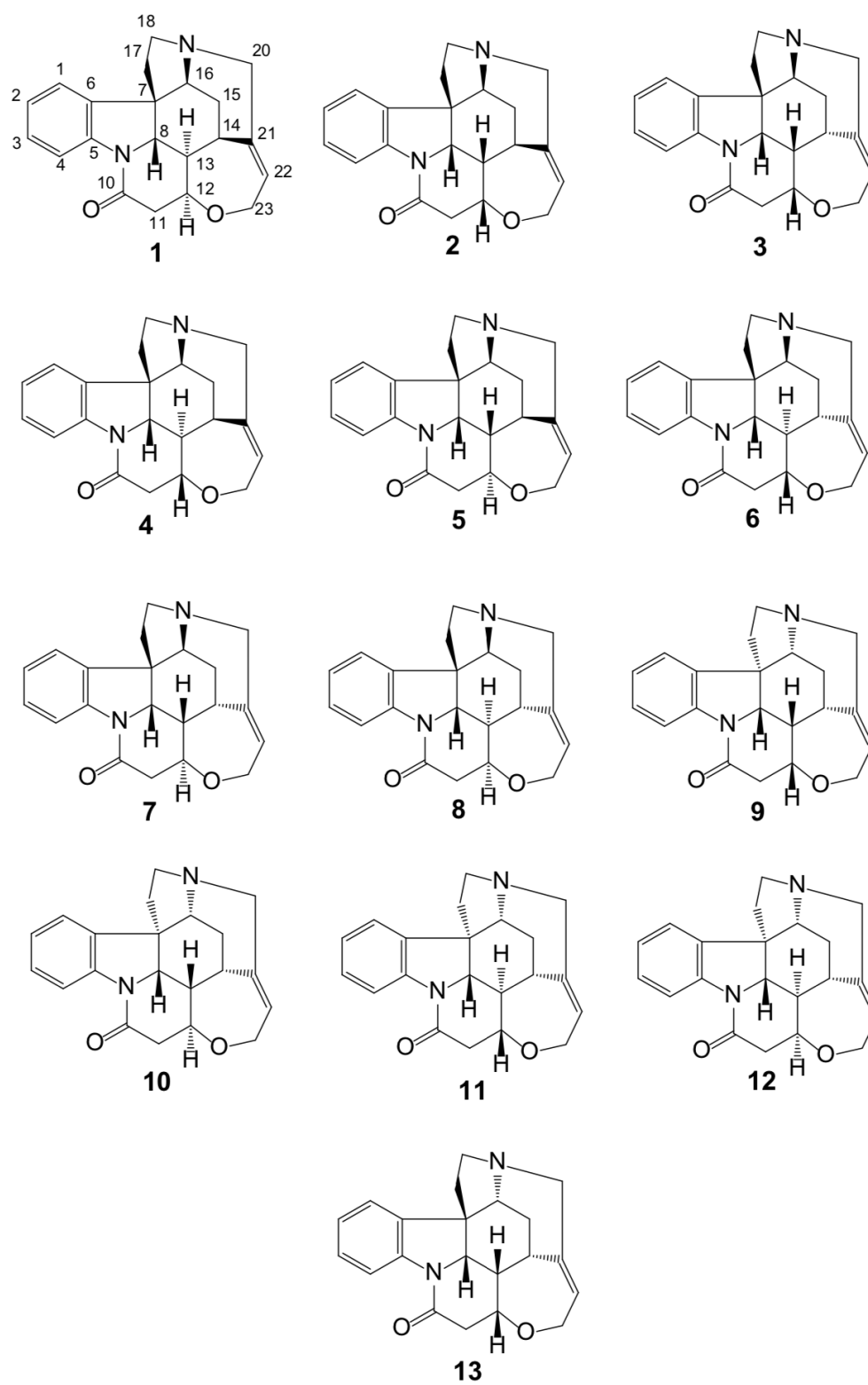


Figure S18 The 13 Energetically viable Strychnine diastereomers used for the IMPRESSION validation?

S6 Large errors

The largest 5 individual errors between DFT and machine learning for the test set are shown here, for each of the parameters $\delta^{13}\text{C}$, $\delta^1\text{H}$, and $^1J_{\text{CH}}$.

S6.1 ^1H chemical shifts

Mol ID	Atom ID	Error [ppm]	DFT [ppm]	ML [ppm]	Variance [ppm]
YEHWUD	36	11.22	-4.27	6.96	0.63
BEDFUM	6	3.22	3.21	6.42	0.18
IQIKOI	21	2.15	5.34	7.50	0.0023
AROKUN	19	2.01	6.83	8.84	0.0025
WAWQUH	37	1.94	0.76	2.70	0.014

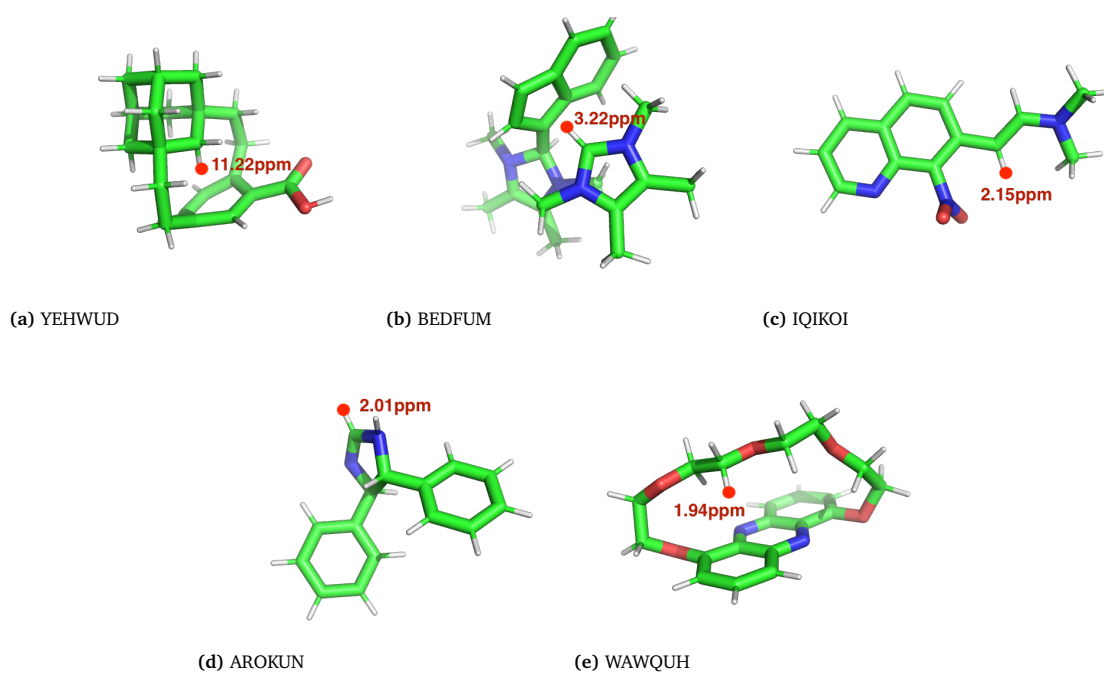
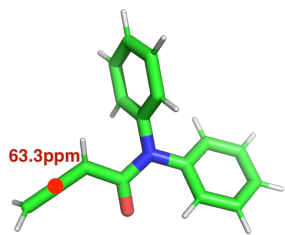


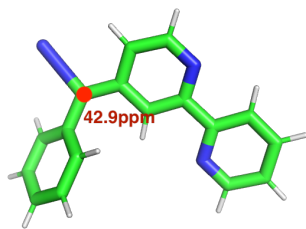
Figure S19 Biggest errors in ^1H prediction.

S6.2 ^{13}C chemical shifts

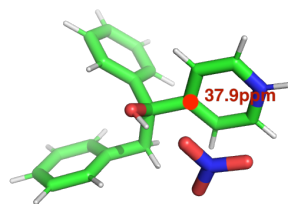
Mol ID	Atom ID	Error [ppm]	DFT [ppm]	ML [ppm]	Variance [ppm]
DOVWAM	4	-63.33	217.35	154.02	353.15
QUFCEZ	15	42.92	60.82	103.75	45.22
RACGEJ	10	-37.87	180.27	142.40	2.02
BEHWER	5	35.31	115.95	151.26	2.89
QOMVUK	1	32.90	92.98	125.37	8.41



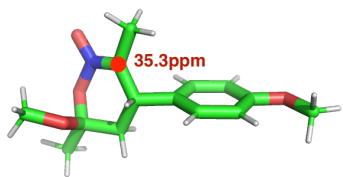
(a) DOVWAM



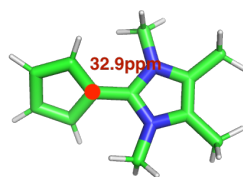
(b) QUFCEZ



(c) RACGEJ



(d) BEHWER



(e) QOMVUK

Figure S20 Biggest errors in ^{13}C prediction.

S6.3 $^1J_{CH}$ coupling constant

Mol ID	1H Atom ID	^{13}C Atom ID	Error [Hz]	DFT [Hz]	ML [Hz]	Variance [Hz]
YEHWUD	10	36	24.63	116.31	140.94	365.70
JOTKIM01	50	51	24.40	194.51	218.91	8.52
ZEYLAS	61	70	-18.31	182.64	164.35	3.49
IDURLJ	13	14	-13.37	171.56	158.19	0.13
FEMXOK	7	19	12.13	144.21	156.35	1.01

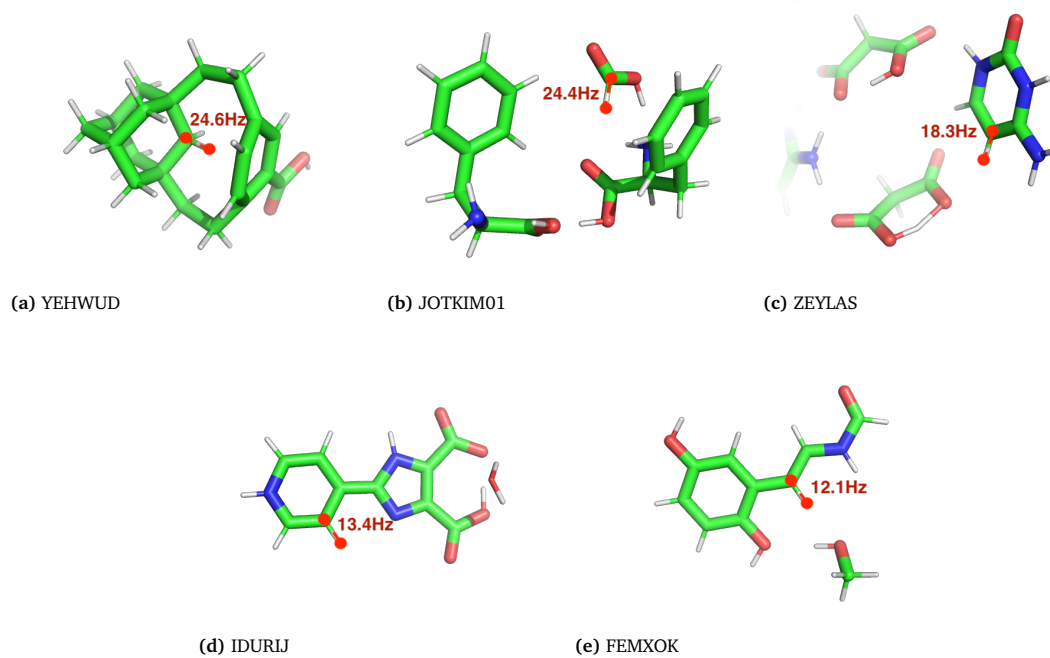


Figure S21 Biggest errors in $^1J_{CH}$ prediction.

S7 Gaussian input files

Example input files for the Gaussian09 software are included here.

```
%Chk=Mol00001_OPT
%NoSave
%mem=26GB
%NProcShared=8
# opt=tight mpw1pw91/6-311g(d,p) integral=ultrafine MaxDisk=50GB

Mol00001 OPT

0 1
C -0.03886 1.59169 0.09099
C -0.05003 0.06176 -0.01881
O 0.67385 -0.53818 1.05146
C -1.48763 -0.47708 -0.00138
O -1.98929 -0.21555 1.30848
C 0.65858 -0.42520 -1.30698
O -0.00173 0.02276 -2.45802
C 2.11254 0.00797 -1.33359
O 2.55982 0.61959 -2.27613
H 0.97884 1.95353 0.26194
H -0.42422 2.04115 -0.82812
H -0.66421 1.91188 0.92773
H 0.07032 -0.53935 1.80579
```

Figure S22 Gaussian Optimisation Input File

```
%mem=26GB
NProcShared=8
#T nmr(giao,spinspin,mixed)wb97xd/6-311g(d,p) maxdisk=50GB

Mol00001 NMR

0 1
C -0.03886 1.59169 0.09099
C -0.05003 0.06176 -0.01881
O 0.67385 -0.53818 1.05146
C -1.48763 -0.47708 -0.00138
O -1.98929 -0.21555 1.30848
C 0.65858 -0.42520 -1.30698
O -0.00173 0.02276 -2.45802
C 2.11254 0.00797 -1.33359
O 2.55982 0.61959 -2.27613
H 0.97884 1.95353 0.26194
H -0.42422 2.04115 -0.82812
H -0.66421 1.91188 0.92773
H 0.07032 -0.53935 1.80579
```

Figure S23 Gaussian NMR Calculation Input File

Training Data CSD Reference Names

ABIVIQ	BOPKAS	CUDSAX	EFUMUP	FOFQOG
ABOTOC	BOTMUT	CUGLIA	EGAXAL	FOGBIN
ACALIZ	BOVCEW	CUKCAM21	EGOTAW	FOGKIW
ACTOLD05	BOVJOL	CUKSEG	EGUQAY	FOLQUT
ADAZUB	BUBPAQ	CUSFEC	EHAJUS	FOMZUD
ADIDUN	BUCLUI	CUVBIF	EHYID	FOQNUV
ADOXEZ	BUDHOZ	CUZPAP	EHNPRG	FOTYAP
AFIFAX01	BUGKIX01	CYTOSM13	EKAHOO01	FOVVIV01
AFIGIG	BUGMOG	DAFLIH	ELENEQ	FOWPOW
AFIHOO	BULHIZ	DAJXUI	ELOKIB	FRANAC04
AFUNAR	BULKID	DAQJOV	ELUGOI	FUCVOO
AGAVOU	BUYZUQ01	DAWYEI	EMAQEQ	FUGXIO
AHMVAL	BZCPRO	DEBDIX04	ENIJIV	FULJON
AHUHUH	BZPHAN01	DEBGIB	EREVUS	FULZIV
AHUYUX	CACWAG	DEGREM	ERISII	FUMTOY
AJAPIL01	CAGMIJ	DENPUH	ESTILO03	FUNGAX
AKIGAE	CAHBUL	DETLAQ	ESUQOZ	FUQZEY
AMMCHC11	CANPEM	DETPAU	ESUROZ	FUTWAU
AMUVIP	CASTEV	DEVCIR	ETIROQ	GAMLOV
ANIZUT	CATKAL	DEYTIL01	EVAWEE	GAQLOB
APUREI01	CAXLIX	DIBENZ13	EVAWIJ	GASNEU03
AQUWOY	CBUDCX02	DIBNEH	EVICUJ	GATVED
ARIWAB	CEBKEZ	DICRUD	EVIMUR	GAZPII
ATEZOO	CEBKEZ06	DIFQEP	EVOGOM	GEFLEK
ATOGIB	CEBQIK	DIGGOP	EVOJIK	GEFQIS
ATUJEF	CEFB0H	DIKFEJ	EWODEA01	GEHHEZ
AVALAM	CEGREL	DISJEW	EXOQEO	GELDEI01
AWIZUB	CEHZIY	DIZMOQ	EYIKUS	GENFUA
AWOTAH	CEKPIR	DLALNI14	EYOGEG	GEYTIN
AXADAF	CEKYAS	DLHTDA10	EZUJIU	GICCEA
AXADUZ	CELRAP	DLTYRS	EZUTIC	GILKIW01
AXEHAO01	CEMBED	DMTCUN10	FABVUC	GIMGIU
AXMQOL	CEPKIS	DMXNPY	FACQUV	GITNEE
AYEROL	CIBFEA	DNPOL	FACWUC	GIVHOJ
AZIWUD	CIFSIV	DODWOI	FAFXUF	GOCCOS
BAFDIV	CIGJUX	DOFGEK	FAHPAH	GODSOH
BAJYOB	CIKBUU	DOKVUV01	FAMFII	GOJVUY
BANJOQ	CIPBAF	DOPSAC	FASZOP	GUFXOV
BAPQOA	CIQHOA	DOQDET	FATBEI	GUHXOY01
BAPYAU	CIQYAD	DOSZES	FAVYIN	GUKXIT
BASDOO	CIRGOB	DOTPOS	FAZRED	GULDIA
BASHUA	CISXOT	DOVGUR	FECQAF	GUMMOZ01
BATVEY	CITQAY	DOYVUK	FEFYEX	GUYBOR01
BAVZEE	CIXGOF	DUCWAA	FEGFIG	HAFDIC
BAYZUW	CMXMCH	DUDDOV	FEHLEL	HAHVYI
BEDJOM	COCPAN	DUDKUJ	FEKDUU	HAKWUN
BEFJAY	COFGUA	DUFVEG	FEQFIT	HALNEP
BEJTEP	COFNUI	DULJEA	FERTON	HALVAT
BELHAB01	COGMOB	DUNLAA	FESNOG	HAMDOP
BEMZAV	COLYIN	DUNSAH	FESQAX	HATXIJ
BEXNUO	COMXOR	DUNTOV	FEVHEV	HAWTEF
BEZREF	CONNUP	DUSJAD	FEWSEH	HDPDXZ
BIBXIT02	COTMEE	DUSWIY	FICLEK	HELYOM01
BICVIS01	COWLUX	DUTTAN10	FICTOC	HEQWOQ
BIFFAZ	COXXIY	EBIWEU	FIHNUH01	HEVDIW
BIWZOX	COYREO	ECASAC	FIJQAQ	HEXVAI
BOAYPI	COYSIS	ECIPIR	FIKCAE	HIFGEJ
BOCHIL	CTOGBS20	ECMPCA	FIYBEU	HIFPIX
BOGFUA	CTPROL10	EDEKOQ	FNPEYO	HIFQET
BOMBEK	CUDDUB	EFIKOT01	FOCBEF	HIGCIK

Training Data CSD Reference Names

HIYHAY	KADDIE	MAMKAO	NEFHOY	PENBUH
HMCNSP	KAGZIE	MAPLIZ01	NEMZAG	PENTYN
HNOBCH	KAMROH	MAQWIM16	NEPXIR06	PEPGEW
HOCFUL	KATKIA	MATGOG	NEPXOX	PEXFUT
HOMCOD	KAVCOC	MATPEC	NESZOB	PEXLAH
HOPKUT	KAYHIE	MATVAE	NETIND01	PEZFEG01
HOQSIQ	KEDRER	MAXDUL	NEWREN	PHTHAC02
HOVFUT	KEMHAL	MECZID	NEXMOT	PHTHAC06
HOWWOH	KESTAD	MEDLEN	NIFBEJ	PIBGOX
HOZBII	KIBKAJ	MEGNES	NIFJOB	PIGROM01
HOZGAG	KIGQIA	MEHPIB	NIFRAX	PIGTAC
HURLAI	KIHxUW	MELVAA	NIHNEY	PINVOX
HXMTAM10	KIMSUU01	MENNAV	NIJKEX	PINYIW
HXOCTM	KINGUJ	MENSEE	NINWEO	PIPINE01
IBUYIQ	KIXROA	MEQFAS	NIPYAZ	PIPINE11
ICAPOR07	KIZVEV	MESYIS	NISMAD	PITQIS01
ICEMIO01	KOCKET01	METAMIO2	NIVJAE	POBDER
ICOYEE	KOKLIH	MEWROX	NIVMIQ	POBSAB
IDILUD01	KONTIQ01	MEYCIC	NIYWID	POQVUO
IGENOZ	KOPBAS	MEYTUH	NOFYEM	POQWOJ
IHANAG	KOTJAE	MEYWOC	NOQBUQ	PORROE
IHOQUT	KOVFUW	MEZHEG	NOVDOR	POSJAI
IJIHOA	KOWCAC	MIDXIH	NUBLOL	POVJAL
ILAJIQ	KOXBEE	MIHZUZ	NUHFEB	POZWUW
ILIMEV02	KUGKAZ	MIMREG	NUKJIO	PUDDUP
IMUXOF	KUKCUP	MIMTAE	NUKXEX	PUQNUK
INACET03	KUQFUY	MINGAR	NUPQEU	PUQTAW
IQIDIV	KUVBEI	MIPYAL	NUQHIR	PUYTAE
IQIZAK	KUVKES	MIQNEF	NUYWIP	QACVAT
IQOROW	KUVWON01	MIVTUG	OBOWOU	QAHSOI
IQUFUX01	KUWZOS	MIWQIS	OCEHIP01	QAJBUZ
ITAFEP	KUXJIY	MIXWEX	OCOPOL	QAKJUJ
ITIKEB	KUYNOH	MNPYDO10	OGOXEP	QAKMOG
ITUVOI	LACVAM	MOBXAC	OHIWUX	QALZUA
IVAKAS	LAFHEH	MOFCOA	OJAQOH	QANQUR
IVEREH	LAVCET	MOGYIR	OLOJAB	QAPJIA
IVIDAS	LEGXUS	MOLQUB	OLOREM	QAPNAZ
IVIHAY	LEHJAM	MOYKUG	OMCHDO	QAPVOT
IXOYEA	LEMVEH	MTHPRG	OMOMOS	QATVIS
IYASUW	LEPPIF	MTYROS01	ONILAZ	QAZMIP
JABKUV	LERJAV	MUGDID	OPOZAW	QEBBUW
JAPBIO	LESCET	MUHZUM	OQUHEP	QECHEO
JAWCIW	LEZJUV	MUKBUR	ORIDAW	QEPNUW
JAXHEW	LGLUAC13	MULBIE	OTAKEB01	QEYRER
JECNUD	LIHMOG	MUNWUP	OWOHAL01	QIKJIF
JEDTIV	LILDEP	MUVCAI	OXOFMB	QIMKIG03
JEGTUN	LILJOG	MVAHIV	OZICAC	QIQYIA
JEXBOE	LIWFEC	NACGOP	PABBIF	QIRLUA
JINHET	LIYPEO	NADVIX	PADTIX	QIWGEJ
JOC DAG	LOCVEE	NAFHOR	PADXOJ	QIWMUG
JONQOU	LOKDEW	NAMZAC	PAFGUA	QOVREZ01
JOTBAV	LOMHOK	NAMZEG	PAGLEO	QUOREM
JOYGEJ	LOMNUY	NAPHTA23	PAGWIG	QUVPOO
JOZYUU	LOSMOW	NAPTYR11	PAJDOW	QUWJOJ
JUMCEB	LOVCAC	NASRUV	PAJVOO	QUYJUQ
JUNJIN	LUPGAG	NATNAA	PARHAR	RAFINO01
JUPJAH	LUQSOG	NAXRUC	PAXCEX	RALQUR
JUSQUL	LUQYIG	NAYPAF	PAYJEH	RAMZEL
KABHED	LURVUR	NAYZOD	PEFSID	RAYXEU
KACNIN	LUVPEX	NEDYEA	PEGLUL	RAYXOH

Training Data CSD Reference Names

REBXON	SUPKET	URAWEQ	WOBLAA	YEXZIM01
REDYAB	SUSYAI01	URESOB	WOBWUF01	YIDPEG
REGFER	SUVCUJ	USUZUF	WOGQEO	YIDPIM
REGKIX01	SUXCAQ	UTAGAZ	WOJGUX	YIFWAM
REGYEJ	SUXROS	UTEJIO	WOJHAG	YIGSUE
RELCUH	SUZJAZ	UTIHOF	WOKPER05	YIHHON16
REYCII	TABBOQ	UVIMES	WOLNIW	YILYOJ
REZJUC	TABNIV	UWAGEB	WOZPUW	YOGSIY
RIFBUE	TACRIB02	UXICAH	WUCJOV	YOKYOO
RIGVEJ	TAHMOE	UYIREB	WUKLAP	YONBOT
RIQWIZ	TALHAR	UYUDUO	WUSQUY	YOPLIY10
RIWNEQ	TALNAV01	UZUHED	WUWMEG	YOWRAF
RIXXOM	TAMLID	VACLAM02	WUYMUZ	YOXGIB
RIZWUS	TANBEP	VAJVOU	XAKLUR	YUCQUJ
ROLVEV	TANTEK	VAPCEW	XAVMUE	YUDLAM
ROSLAO	TAPCIW	VAWJAG	XAVZOJ	YUDMOZ
RUCFAX	TARGEb	VAXLAJ	XAXHOW	YUDPAQ
RUGCED	TARGUO	VEBWEH	XAYDIK	YUFYED
RUGQOA	TATNEI	VECSAZ	XAZQOF	YUHTEA03
RUJQOE	TECQEX	VEFPIF	XAZROH	YUHTOK
RUJSAS	TEGVUW	VESHUX	XEBYUA	YUNTOR
RURRAY	TEJREG	VEXCUW	XEDNAX	YUNYIR
RUVSAC	TEKSOR	VEZNOF	XEDTEG	YUQCUJ
RUWJAU	TELKAZ	VIBZUB	XEHTUZ	YUQMED
RUWMAX	TENMIK	VIDFEV	XEMDAX	ZAJHOH
RUWQIK	TEPHME02	VIGWOY	XENLAE	ZAJVAK
RUZXIU	TEVLIQ	VIGXAK	XETMAL	ZETHUD
SADJEM	TICBUD	VIHBIZ	XEVCEH	ZEWPUM
SADXOL	TIHBAO	VOFSEP	XEWNES	ZIFKEG
SAGQUO	TIMHED	VOKXOJ	XEXQOH01	ZILQOA01
SAHCOV	TIQNIQ	VOLKIS	XEYRIE	ZIYSIL
SAHZAF	TIQWOG	VUDKIP	XEZYIK	ZODXEV
SAKJUM	TIXPOF	VUFGEI01	XIJFEB	ZOFCUU
SANWEJ	TMXSTQ10	VUFSEU	XIMCOL	ZOLBUX
SAPHAU	TOHVIW	VUFWAV	XIMJAE	ZONYUY
SARJED	TOPROG	VUKFOY	XINJIN	ZOZTOX
SAWHUV	TOPSEW	VUNFUF	XISHOY	ZUPGIA10
SAWJUX	TOVSUS02	VUPHIZ	XIVVAA	ZUPGUM
SAYTAN	TPHETY01	VUTBUI	XIWREA02	ZUPHAT
SAYWOG	TUCJEI	VUTNAB	XOBGAY	ZUQVOY
SAZLAH	TUCNUC	VUZQOX	XOGWAR	ZZZLUK05
SECTIF	TUJJEP	WABTAU	XOGXEX	ZZZMBS02
SEDMOD	TULDAH	WACZUX	XOMJIS	
SEHNAW01	TUNCOW	WADGEO01	XOWDAQ	
SEJWOT	TUNTUT	WADQID	XUHPIB	
SELKEB	TUSQUU	WAGBEO	XUPYIR	
SEQREN	TUWCEU	WALNEC	XUVSUE	
SIQQEP	UBEBAG	WANVEP	XUYZIC	
SITCUU	UBUPEM	WAQNUZ01	YAGJEX	
SIVJOY	UCOMOO	WAZMAL	YAMHID01	
SIWDEH	UCOQAE	WECXUZ	YAPBUO	
SIYYUU	UCUZOJ	WESVIZ	YAPZEU	
SOPLEO	UDEHER	WEWTUP	YAQWAR	
SOXHAA	UFAGOY	WIBWIN	YARDUQ	
SUCACB12	UHADOX	WIBXUA	YAWWAU01	
SUCANH12	UKUTUP	WIFZOC	YAYDIN	
SUCROS47	UPACUK	WIPHAG	YEJPAG	
SUCTAN	UPADOG	WIVYUV	YEJZES	
SUFGAB	UQIMUE	WIYDUF	YEKVEQ	
SUHYIE	URAHIF	WIZZAI	YENLAF	

Testing Data CSD Reference Names

ACRDIN07	DAFTAF	GADSIO	KETYUF	OGIMIC
AFIQUC	DAJZEU	GADVAJ	KOFKAR	OHEWOP
AHATEK	DASNIV	GAQJUF	KOGWUZ	OJICUF
AHOWOL	DENXUP02	GASXON	KOJTOT	OMABEK
AHOXOL	DILDUZ	GAWFEQ	KOTMUB	OMSTER01
AJIXUM	DILKIT	GIDHUW	KUJZIY	ONBZAM
AKUBIT	DITZOX	GIXKOP	KUTKAL	OPIZAQ
ALEXEW	DIWWEN	GIZFEB	KUYWEH	OWIWUN
ALOSEZ	DIZWEQ	GIZRUE	KUZJIA	OXAROV
AMEXOH	DOHPEV	GOVQOX	KUZQIG	OXUJUN
AMUQOQ	DOLBIR10	GUCJUK	LADNEL	PACWAU
ANAHII	DOMNEY	GUFYOX	LAFHEH	PANLEZ10
ANOSAY	DORKOK	GUJGEX	LAVSIL	PEDHAJ
APODUG	DOTFOI	GUTZOM	LEVSIO	PEFGIS
APUPIK	DOVWAM	HABNED	LILDEP	PELXAG10
AQAGII	DUTKOU	HAMTIZ	LIXQEO	PEPLAX
AQEYAW	DUZLUF	HAXREE	LIZHEJ	PETRAH
AROKUN	DXCYTD	HECNOS	LOPLUZ	PEWNIQ
ARONOM	EABZBU	HESTOO	LUDZIT	PEXPEN
ARUZUK	EBAXOW	HIMSUS	LUQDOS	PHBZAC01
ASPARM10	EBOVEX	HISNII	LUXSAY	PIHBOZ
AWAVEZ	ECODUV	HIWYIV	MAHPUJ	PIJREF
AXADAF	EDAXOW	HIZHOP	MALSOH	PILFIB
AXAWIG	EDIZUM	HODKEQ	MAQWIM23	POHCAS
AXOSOW03	EFIBAX	HODLOC	MATQOO	POKKAD10
AYUNEO	EHAHAY	HOMKIF	MEHLER	POLJEF
AZIDES	EKAHOP	HOMZUG	MEHNAP	PRMDIN05
BAJCIY03	EKAWAQ	HONKEC	MEJDOU	PUMQEV
BAPPUF	EKOGAO	HUDHEU	MEJQEY	PUNFAH
BAQNEM	ELAWIX	HUDYUA	MELAMI05	PUPBAD01
BASNOZ	EMEFOT	HUVWOL	MENDAL01	PUWNIG
BAWRAT	EMIPUM	HUYYOP	MESQOR	PYAZAC
BAYPAT	EMISUQ	IBEHII	MEYBIB	QAKDAJ
BEDFUM	EMODUG	IBOPIA	MISDAT	QAMKEW
BEDLEB01	ENIMET	IDUJEW	MOBNUM	QECNAP
BEGDIB01	EPHEDR01	IDURIJ	MODXUZ	QEPRIO
BEHWER	ESESEA	IJEZUS	MOSLAI	QEXKUA
BERSOG	EVIHUM02	INAVIC	MOTNUF	QIYLAM
BIKNUE	EVILEB	IPINIE	MUBBAN	QOMVUK
BIXQEF	EVINII	IQIKOI	MUJGEE	QQQAMS02
BOLGOZ	EVIQEF	IQIZEO	MUTWON	QUFCEZ
BOMSIH	EWOBIB	IQUBZA	NAJLUF	QUFJUY
BOPJAS	EXEWEJ	IQULUC	NANJIW	QUWFIZ
BUFNEV01	EXEYUD	IROZII	NAPTPR	RACGEJ
BUGQUQ	EXUVUP	ISIJIE	NASZAJ	RAKTOO
BUMNOM	EYASAZ	ITINEG	NBZOAC11	RAVFOK
BUZJIR	EZISUC	ITIREI	NCUBEB10	RECYIH
BZAMID08	FACZIU	IVABEO	NEQPEG	REKMEZ
BZTROP11	FADHOJ	IVEZAK	NEVDON	RICTIG
CAZCOX	FAHLAB	IYASUW	NEZFON	RIHFIY
CBMZPN21	FAHXUH	IZAKOK	NIQTAJ	RIMHEC
CIKSAQ	FAJDEC	JESHIZ	NORFUW	RIZBAF
CINCHO10	FELDOR	JIPCUG10	NUKSAO	ROGRIQ
COCYAW	FEMGAF	JOQTUE	NUQLES	ROHJED
COLBAG	FEMXOK	JOTKIM01	NURZOP	ROJHOP
CORTPY	FEPTID	JULGOO	OCATOC	ROJXOD
COWPUZ	FEZLUT	KABKIJ	OCAWOF	RUCNOU
COYBOJ	FIHLEO	KAHJEK	OCIPAR	RUKTAU
CUTCUQ	FOSLEG	KAKHEL	ODOROO	RULDAF
CXMTUN	FUPWES	KEMFIS	OFEVOL	RULHOX

Testing Data CSD Reference Names

RUVPIJ	WIFQEI
SAJCAJ	WIHBEW
SATPEI02	WIQZOL
SATPUZ	WOBRIP
SAVREN	WOKJOV
SAWVET	WUCVIB
SAZFOO	XABFUE
SEBVAW	XAQTUF
SEFNOG	XASHUW
SENKUR	XAZYIG
SEYCUU	XEZFUF
SIGSAD	XIMGAB
SIHCES	XINHIL
SIHZAM	XIYTIJ
SOGCUN	XIZVAD
SORFIQ	XOFFEF
SUHFEH	XOHMAI
SUKNIW02	XOWJUP
SUWKEC	XUJKUK
SUYIIV	XULNOI
TAJSOM	XUVBAT
TAVJAD	YAZDEI
TEMKAZ	YEGGIA
TESDOL	YEHWUD
THYDIN05	YERTIZ01
TICLIC	YIDTIQ
TIWZUV	YIMPOB
TOPRIB	YIPPOC
TOPXUT	YIXPUR
UBUXOG	YOCWUK
UCANIV	YODPAJ
UJUKIT	YOFTOE
UKUROJ	YOWYOY02
UMUKUJ	YOXRIO
UNAMOL	YUNYUC
UNURIF	ZATDOP
UNUVEF	ZAYPOE
UQAMIK	ZEBXOV
UQOLIW	ZEMNAG
UWEZED	ZEYLAS
UWOCAM	ZIGBAS
VAFFAV	ZIKQIT
VANFEV	ZIWMOJ
VASLOR	ZIYYUD
VEQMUA	ZOFNUD
VETJIO	ZOSVEI
VEZCUY	ZOXYOA
VIDDAO	ZOYMOP07
VIDMAX02	ZZZBPY10
VILPUB	ZZZFFY01
VOCHUR	
VOGDIE	
VONNOB	
VOXNOL	
VUDDUV	
VUHZEE	
WAFBIQ	
WAWQUH	
WECZEJ	
WEVVEZ	

S9 Full Gaussian reference

Gaussian 09, Revision D.01, M. J. Frisch, G. W. Trucks, H. B. Schlegel, G. E. Scuseria, M. A. Robb, J. R. Cheeseman, G. Scalmani, V. Barone, G. A. Petersson, H. Nakatsuji, X. Li, M. Caricato, A. Marenich, J. Bloino, B. G. Janesko, R. Gomperts, B. Mennucci, H. P. Hratchian, J. V. Ortiz, A. F. Izmaylov, J. L. Sonnenberg, D. Williams-Young, F. Ding, F. Lipparini, F. Egidi, J. Goings, B. Peng, A. Petrone, T. Henderson, D. Ranasinghe, V. G. Zakrzewski, J. Gao, N. Rega, G. Zheng, W. Liang, M. Hada, M. Ehara, K. Toyota, R. Fukuda, J. Hasegawa, M. Ishida, T. Nakajima, Y. Honda, O. Kitao, H. Nakai, T. Vreven, K. Throssell, J. A. Montgomery, Jr., J. E. Peralta, F. Ogliaro, M. Bearpark, J. J. Heyd, E. Brothers, K. N. Kudin, V. N. Staroverov, T. Keith, R. Kobayashi, J. Normand, K. Raghavachari, A. Rendell, J. C. Burant, S. S. Iyengar, J. Tomasi, M. Cossi, J. M. Millam, M. Klene, C. Adamo, R. Cammi, J. W. Ochterski, R. L. Martin, K. Morokuma, O. Farkas, J. B. Foresman, and D. J. Fox, Gaussian, Inc., Wallingford CT, 2016.